# Physics-Constrained Gaussian Process Model for Prediction of Hydrodynamic Interactions Between Wave Energy Converters in an Array

Min Li[a], Gaofeng Jia[a,*], Hussam Mahmoud[a], Yi-Hsiang Yu[b], Nathan Tom[c]

[a]*Department of Civil and Environmental Engineering, Colorado State University, Fort Collins, CO, USA*
[b]*National Yang Ming Chiao Tung University, Hsinchu, Taiwan*
[c]*National Renewable Energy Laboratory, Golden, CO, USA*

**Abstract**

To improve the efficiency of wave farms and achieve maximum power generation, the layout of wave energy converters (WECs) in an array needs to be carefully designed so that the hydrodynamic interactions can be positively exploited. For this, the hydrodynamic characteristics of the WEC array in different layouts need to be calculated. However, such calculations using numerical models usually entail significant computational cost, especially for large arrays of WECs. To address the computational challenge, a physics-constrained Gaussian process (GP) model is proposed to replace the original expensive numerical model and predict the hydrodynamic characteristics of the WECs for any array layout. By exploring the relationship between the WEC array (i.e., the input) and different hydrodynamic characteristics (i.e., the output), we summarize a set of physical constraints/features, including invariance, symmetry, and additivity. This prior knowledge about the input-output relationship is then directly embedded in the constructed GP model through the design of physics-constrained kernels. In particular, a double-sum invariant kernel is first developed to incorporate the invariance and symmetry features, and then an additive kernel is developed to incorporate the additive feature of the problem. The invariant kernel and the additive kernel are then integrated to construct the physics-constrained GP model. Compared to the standard GP model, the proposed physics-constrained GP models require less training data to achieve the desired accuracy in predicting the hydrodynamic characteristics and are also less vulnerable to the curse of dimensionality (i.e., good scalability for large arrays) due to the use of an additive kernel. The efficiency, accuracy, and scalability of the proposed approach are demonstrated through an application to predict the hydrodynamic characteristics for WEC arrays of different sizes and layouts.

*Keywords:* Wave energy converters, Hydrodynamic characteristics, Physical constraints, Gaussian process model, Kernel design

## 1. Introduction

According to the U.S. Department of Energy, the estimated total renewable wave energy resource in the United States has the potential to power more than 100 million homes each year [1]. The deployment

*Corresponding author

of wave energy converters (WECs) in large-scale arrays, also known as wave farms, offers great prospects for harnessing such renewable wave energy and facilitating electrical power transmission. Unlike the single-WEC configuration, a wave farm typically involves complex physical laws (i.e., WECs interact with scattered and radiated waves), and the hydrodynamic interactions between neighboring WECs could have a significant impact on the total power generation of the wave farm. By arranging the positions of WECs in array properly, the total power generation can be greater than the power generated by the same number of isolated devices [2, 3]. In order to improve the efficiency of wave farms and achieve maximum power generation, the layout of WECs needs to be carefully designed so that the hydrodynamic interactions can be positively exploited. Therefore, hydrodynamic modeling has drawn extensive attention in this field.

Most previous research on modeling hydrodynamic interaction has been conducted based on linear potential flow theory [4], and various numerical methods have been proposed within this context for calculating hydrodynamic interactions within arrays of WECs [5]. The main methods can be classified into two classes: (i) analytical or semi-analytical methods, such as point-absorber approximation [6], plane-wave approximation [7], and the multi-scattering method [8]; and (ii) numerical methods, such as the boundary element method and finite element method. However, if high accuracy is desired, the computational efforts may still be burdensome, especially when the number of WECs is large and higher-fidelity models are used. Moreover, additional challenges also arise when dealing with problems such as uncertainty quantification and design optimization, which typically require a large number of model evaluations.

To address the above computational challenges, this paper proposes a surrogate-model-based approach for predicting hydrodynamic interactions between WECs. Surrogate models have been extensively used to approximate the input-output relationship for computationally expensive models in various disciplines. They are trained using a data-driven approach, and the training data are obtained by evaluating the expensive models over a number of input points. The computational efficiency of surrogate models is greatly increased. Therefore, once trained, the original expensive models can be replaced by the surrogate models for subsequent analysis and design where repeated model evaluations are needed. Among various surrogate models proposed in the literature, the Gaussian process (GP) model [9, 10] has been gaining popularity due to its flexibility in modeling complex functions and its ability to provide closed-form predictive distributions. Therefore, this paper will focus on the GP model.

The application of surrogate models, or more generally machine learning models, has been explored by researchers in the field of wave energy converters. A kriging surrogate model based approach was proposed in [11], based on which the layout design of arrays with different number of WECs was performed with high efficiency. Neshat et al. [12] proposed an adaptive neuro-surrogate-based approach for achieving optimal placement of wave energy converters, where the total wave farm energy was predicted by a trained recurrent neural network in stead of calculated using time-consuming computation. However, the effectiveness and efficiency of these approaches were demonstrated through application in arrays with limited/small number of WECs (e.g., 5 buoys in [11] and 16 buoys in [12]), and their scalability to larger arrays may still need

to be investigated. Sarkar et al. [13] introduced a machine learning based method for the optimization of large-scale arrays with oscillating wave surge converters. By decomposing the whole array into small clusters and approximating the performance of the clusters using Gaussian process regression, the proposed approach is able to efficiently optimize large arrays. However, the trade-off for scalability of this approach is to restrict the hydrodynamic interaction between the nearest neighbors of WECs. Overall, these surrogate based methods focus on directly predicting power output of the wave energy converter arrays, while an alternative option is to predict the intermediate variable (e.g., hydrodynamic interactions) and compute the power generation by using the predicted hydrodynamic interactions [14]. The latter option may offer the benefit of constructing more accurate surrogate models with less training data since the underlying input-output relationship is expected to be less complex than the former option. To the authors' best knowledge, little research has investigated the prediction of hydrodynamic interactions using surrogate models. The main difficulties are twofold. First, the standard way of building a surrogate model fails to incorporate available prior physical knowledge about the problem or input-output relationship. The direct surrogate modeling option is to take the layout of a WEC array (i.e., represented by a vector consisting of the coordinates of the WECs) as the model input, and the hydrodynamic characteristics as the model output. However, the hydrodynamic characteristics could be permutation-invariant with respect to the ordering of the WECs given an array layout, or they could be symmetric with respect to the axes. In addition, the WEC interaction problem is similar to the classical many-body interaction problem [14], and the hydrodynamic characteristics can demonstrate the additivity feature. Directly taking the coordinates as inputs and applying commonly used product kernels for training the GP model cannot incorporate prior knowledge into the surrogate modeling. Instead, these features (i.e., invariance, symmetry, and additivity) can only be learned by a large number of training data if directly using the common way to train the surrogate models. However, a lot of times obtaining many training data for the hydrodynamic characteristics is impractical due to the high computational cost of running expensive models (e.g., MS solver or boundary element models). The limited training data typically will lead to lower prediction accuracy and generalization ability of the established surrogate model. Second, as the size of the WEC array increases, there are additional challenges in constructing a surrogate model that stem from the increased input dimension, which typically requires more training data to obtain the desired prediction accuracy (i.e., suffering from curse of dimensionality). However, the computational effort to calculate the hydrodynamic characteristics typically increases significantly with the number of the WECs, which means obtaining training data is more costly. In the end, building surrogate models for prediction of hydrodynamic characteristics becomes a challenging task. To tackle these issues, the most related research is in [14]. They proposed a surrogate-model-based approach to predict the hydrodynamic characteristics of multiple bodies through a hierarchical interaction decomposition method. The key idea is to decompose hydrodynamic characteristics into contributions from clusters with fewer bodies, and then separately build lower-order surrogate models for these components/clusters instead of the total response. This mitigates the curse of dimensionality of surrogate modeling. In addition, by carefully designing the model input ac-

cording to the input-output relationship, these lower-order surrogate models can include the invariance and symmetry principles. Overall, this approach successfully addressed the challenges in surrogate modeling for hydrodynamic analysis by reducing the size of the problem and selecting the proper inputs and outputs.

Alternatively, this paper proposes a physics-constrained GP model to efficiently predict the hydrodynamic characteristics of a WEC array with different layouts. Physics-constrained machine learning aims to introduce physical laws and constraints to lead the model training to produce a physically consistent predictive response [15, 16]. Compared with standard machine learning, physics-constrained models are able to potentially reduce the required training cost [10] and improve the prediction accuracy and generalization ability of the surrogate model under the same number of training data [17]. In the current problem, the prior knowledge about the hydrodynamic characteristics (i.e., invariance, symmetry, and additivity) can be encoded as the physical constraints of the hydrodynamic model. These constraints can be enforced in the surrogate model by adding operations inside the surrogate model that give rise to the desired features. This paper proposes to embed the invariance, symmetry, and additivity in the kernel function to provide more informative prior knowledge for the GP model. In particular, an invariant kernel is first developed to incorporate the invariance and symmetry information, and the established invariant kernel is then integrated into the GP model. This developed invariant kernel enables efficient incorporation of the prior knowledge in the GP model and eliminates the need for handcrafting the input features. Second, taking advantage of the similarity to the classical many-body interaction problem [14], the hydrodynamic characteristics are decomposed to the sum of the outputs from subsystems. Such an additive feature is also regarded as a physical constraint in this paper, and a new kernel is developed to embed the additive feature in the GP model. The kernel exhibits a similar additive feature to the hydrodynamic characteristics and is thus named "additive kernel." Finally, the proposed invariant kernel is combined with the additive kernel to establish an integrated kernel, which is used to construct more informative GP models that explicitly include the known physical constraints on the hydrodynamic characteristics. Compared to the standard GP models, the proposed physics-constrained GP models require less training data to achieve desired accuracy in predicting the hydrodynamic characteristics and are less vulnerable to the curse of dimensionality. It should be noted that the novelty and focus of this work is to design physics-constrained kernels to incorporate prior knowledge about the problem of interest in order to more efficiently train an accurate Gaussian process model. This is in comparison to standard Gaussian process model. Since the hydrodynamic analysis problem shows the permutation invariance, symmetry, and additivity properties, as shown in rent work by Zhang et al. [14], this work tries to incorporate these properties directly in the construction/design of the kernel. It is expected that the proposed approach will have general applicability to other problems as well. The generality of the proposed approach stems from the capability of the kernel to incorporate different prior physical knowledge/constraints (e.g., beyond the permutation invariance, symmetry, and additive properties considered in the current work). For other problems, for example, problems showing periodicity or satisfying partial differential equation, one can potentially update the model by designing corresponding kernels to

incorporate the related knowledge/constraints.

The remainder of this paper is organized as follows. Section 2 presents the hydrodynamic interaction problem for WEC arrays and discusses the computational challenges in calculating hydrodynamic characteristics for arrays with different layouts. Section 3 presents the proposed physics-constrained GP model for efficient predicting hydrodynamic characteristics of WEC arrays with different layouts. Section 4 presents the illustrative example with application to arrays with a different number of WECs and discusses the performance of the proposed approach in terms of prediction accuracy and efficiency. Finally, Section 5 summarizes the research findings.

## 2. Hydrodynamic Interaction Between WECs

### *2.1. Representation of WEC array layout*

Assume the considered WEC array has $N$ identical WECs floating in the water, which are able to oscillate in $M$ modes of motion. Among different configurations for WECs, this paper mainly focuses on cylindrical heave converters, which are heaving floating resonant buoys connected to a power take-off moored to the seafloor. A typical cylindrical heave converter is shown in Figure 1(a). Therefore, the number of oscillating modes $M$ is reduced to 1 here.

A two-dimensional Cartesian coordinate system is defined to express the locations of the WECs. The WECs in the array are under the incident wave propagating along the positive $x$-axis, and the corresponding incident angle is an arbitrary number $\beta$. Figure 1(c) shows an example layout of the array with $N$ WECs, and note that throughout the paper, an array of WECs is numbered as in the figure. Without loss of generality, the leftmost buoy of the array is assumed to be located at the origin of the coordinate system. The layout of the array can then be characterized by the locations of the remaining $N-1$ buoys: $\mathbf{x} = [\bar{x}_2,\ \bar{x}_3,\ \ldots,\ \bar{x}_N,\ \bar{y}_2,\ \bar{y}_3,\ \ldots,\ \bar{y}_N] \in \mathcal{X} \subset \mathbb{R}^{2(N-1)}$, where the pair $(\bar{x}_i, \bar{y}_i)$ represents the coordinates of the $i$th WEC and $\mathcal{X}$ denotes the admissible layout space. For convenience, the layouts of the WEC arrays are transformed into equivalent layouts with all buoys on the right half plane with $\beta = 0$ beforehand, which can be established by rotating the coordinate system and adjusting the origin.

### *2.2. Diffraction and radiation problem*

Following the assumption of classical hydrodynamics (i.e., small displacements, inviscid and incompressible fluid and irrotational flow), the fluid motion can be described by a velocity potential function based on the linear potential theory of waves [20]. By further assuming that all motions are time-harmonic with angular frequency $\omega$, we can extract the time-dependence of the velocity potential [21], and the time-dependent velocity potential function $\Phi$ is then written as

$$\Phi = \mathrm{Re}\left[\phi \cdot e^{-i\omega t}\right] \tag{1}$$

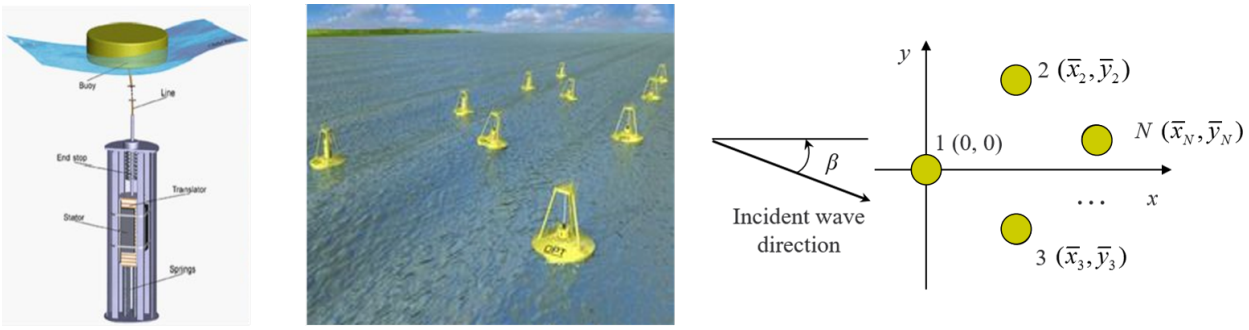


(a) (b) (c)

Figure 1: (a) Wave energy converter (WEC) (adapted from [18]), (b) wave farm (adapted from [19]), and (c) Cartesian representation of an array of $N$ WECs.

where $i = \sqrt{-1}$, and Re[$\cdot$] indicates that the real part is to be taken. $\omega$ is the wave frequency, and should satisfy the dispersion equation $\omega^2 = gk\tanh(kh)$, where $g$ is the gravity acceleration, $k$ is the wave number, and $h$ is the water depth. Due to the linear potential theory of waves, the complex-valued velocity $\phi$ can be expressed by the superposition of the incident wave potential, the scattered wave potential and the radiated wave potential [21]:

$$\phi = \phi_I + \phi_D + \sum_{p=1}^{N} U^{(p)} \phi_R^{(p)} \tag{2}$$

where $\phi_I$ is the incident wave velocity potential, $\phi_D$ describes the velocity potential of the diffracted wave field, $\phi_R^{(p)}$ is the velocity potential of the wave field induced by the oscillation of the $p$th body in the heave motion, and $U^{(p)}$ is the corresponding velocity amplitude. The complex-valued potential $\phi$ must satisfy the Laplace equation within the entire fluid domain, expressed by $\nabla^2\phi = 0$. Also, several boundary conditions should be satisfied, and interested readers are referred to [20, 22] for detailed descriptions of the boundary conditions. By solving this boundary value problem, the diffracted wave potential $\phi_D$ and the radiated wave potential $\phi_R$ can be determined.

In this paper, we are more interested in the hydrodynamic characteristics of the array of WECs, and they can be computed based on the hydrodynamic pressure acting on the devices. More specifically, after the velocity potential in the entire fluid domain is solved, we can calculate the hydrodynamic pressure based on the linearized Bernoulli's equation [23]. Ultimately, the hydrodynamic forces on the WECs may be calculated by integrating the hydrodynamic pressure over the submerged surface of the WECs [21]. More specifically, the wave excitation force on the $p$th body in the direction of heave motion due to the incident and diffracted wave, and the hydrodynamic reaction force on the $p$th body in the direction of heave motion induced by the

oscillation of the $q$th body in the direction of heave motion are written as

$$F^{(p)} = i\omega\rho \int\int_{S_p} (\phi_I + \phi_D)\nu dS \tag{3}$$

$$f^{(pq)} = i\omega\rho \int\int_{S_p} \left[U^{(q)}\phi_R^{(q)}\right] \nu dS \tag{4}$$

where $\rho$ is the fluid density, $S_p$ is the submerged surface of the $p$th body, and $\nu$ is the generalized normal component with respect to the body $p$. It should be noted that the wave reaction force, $f^{(pq)}$, can be reformulated to obtain the radiation-related hydrodynamic characteristics (the added mass coefficient $a^{(pq)}$) and the wave damping coefficient $b^{(pq)}$. The reformulation is written as the following equation:

$$f^{(pq)} = i\omega U^{(q)} \left[a^{(pq)} + i\frac{b^{(pq)}}{\omega}\right] \tag{5}$$

In the end, for a WEC array with $N$ identical buoys (shown in Figure 1(c)), our main purpose is to calculate the hydrodynamic characteristics of the array, including wave excitation force $F^{(p)}$ (corresponding to the diffraction problem), added mass coefficient $a^{(pq)}$, and wave damping coefficient $b^{(pq)}$ (corresponding to the radiation problem), where $p, q = 1, \ldots, N$.

### *2.3. Multiple scattering*

In this paper, the multiple-scattering (MS) method is adopted to obtain the solution of velocity potential of the wave field and calculate the hydrodynamic interaction within the array of WECs due to its versatility in achieving enhanced accuracy. In the first step, this approach requires the solution of the single (isolated) body problem for each body, $p$, within the array. We refer the reader to [1] for more details on the derivation for the case of upright cylindrical bodies under heave oscillation. In the second step, the interaction between the bodies is then addressed by considering the implications to the other bodies (e.g., body $q$) of the diffracted field generated by the initial body, $p$. The accuracy of the MS method is influenced by both the truncation order (i.e., for deriving the solution for a specific body) as well as the interaction order (i.e., for addressing the coupling between the bodies). Further details about the MS approach can be found in [22].

Ultimately, for each considered frequency, $\omega$, the MS method provides the wave excitation forces exerted on each body by the incident wave as well as the added mass and damping coefficients exerted on body $p$ in the direction of heave motion due to the oscillation of of body $q$ in the direction of heave motion. In this paper, we denote $\mathbf{F}(\omega) \in \mathbb{C}^N$ as the response vector relating the incident and diffracted wave to the wave excitation force on each body in the heave direction, and each element of the vector corresponds to $F^{(p)}$. Also, we denote $\mathbf{a}(\omega) \in \mathbb{R}^{N\times N}$ and $\mathbf{b}(\omega) \in \mathbb{R}^{N\times N}$ as the added mass and damping matrices respectively, with the $pq$th element (i.e., $a^{(pq)}$ and $b^{(pq)}$) of these matrices relating the heave oscillations of bodies $p$ and $q$. It is noteworthy to point out that the computational cost of the MS solver can be expensive (i.e., modeling hydrodynamic interactions between WECs takes a lot of computational time), especially when the

number of WECs in the array is large. Considering the significant computational effort in calculation of the hydrodynamic characteristics, typically, one can limit the maximum order of interaction or the the maximum number of eigenfunction series to a relatively small number. Although such implementation gives rise to faster computation of the hydrodynamic characteristics, it trades off accuracy for computational efficiency.

## 3. Physics-Constrained Gaussian Process Model for Predicting Hydrodynamic Characteristics

To alleviate the computational burden in calculating the hydrodynamic characteristics of the WEC array, surrogate modeling can be used. Surrogate models (also frequently referenced as metamodels) can provide an approximate input-output relationship to replace a computationally expensive model, utilizing information within a database of preliminary simulations from that model. Among different surrogate models, this paper focuses on the GP model, which has been gaining popularity due to its high flexibility in approximating complex functions. This section first briefly reviews the GP model and then presents in detail the proposed physics-constrained GP model for predicting hydrodynamic characteristics of a WEC array.

### *3.1. Review of Gaussian process model*

For an unknown function $f$ with input vector $\mathbf{x} \in \mathbb{R}^{n_x}$, given a set of observations a GP model can be adopted to approximate the deterministic function output $y = f(\mathbf{x}) \in \mathbb{R}$. The core principle is to assume the target function $f$ as a realization of a regression model and a zero-mean Gaussian process with covariance or the so-called kernel $\sigma^2 R(\mathbf{x}^i, \mathbf{x}^j)$, where $\sigma^2$ is the variance and $R(\mathbf{x}^i, \mathbf{x}^j)$ is the correlation function.

To create a GP model, the regression basis function and the kernel function need to be specified first. A popular selection for the regression basis function is the polynomial (e.g., a linear or quadratic function of $\mathbf{x}$), and one of the commonly used kernel functions is the squared exponential covariance function. The selection/use of a kernel function introduces some hyperparameters to the GP model, such as the length scale of the correlation function and the variance. Conditioned on the $n$ observations corresponding to the function outputs $\mathbf{Y} = \{y^h; h = 1, \ldots, n\}$ for different inputs $\mathbf{X} = \{\mathbf{x}^h; h = 1, \ldots, n\}$, the predictive distribution of the function output provided by the GP model is

$$f(\mathbf{x})|\mathbf{X}, \mathbf{Y} \sim \mathcal{N}(\bar{f}(\mathbf{x}), \mathbb{V}[f(\mathbf{x})]) \tag{6}$$

where $\mathcal{N}(\cdot)$ represents the Gaussian distribution, and $\bar{f}(\mathbf{x})$ and $\mathbb{V}[f(\mathbf{x})]$ are the predictive mean and the predictive variance, respectively. This predictive variance provides a local estimation of the uncertainty of the model predictions and entails useful information for guiding the selection of the training data. The calibration of the GP model requires a careful selection of the training inputs, $\mathbf{X}$, frequently referenced as design of experiments. It can be established using some space-filling technique such as Latin hypercube sampling (LHS), perhaps augmented through an adaptive refinement to improve the accuracy in target regions [24, 25]. Through the proper tuning of the hyperparameters, the GP model can approximate very complex functions. The optimal selection of the hyperparameters can be based on the maximum likelihood

estimation principle, where the likelihood is defined as the probability of the observations. The development and employment of the GP model is only based on matrix manipulations, and as such is computationally efficient.

### *3.2. Physics-constrained Gaussian process model for predicting hydrodynamic characteristics*

In this problem, GP models are constructed to predict the relationship between the WEC layout and the hydrodynamic characteristics of each buoy. As discussed in Section 2, the layout is characterized by the locations of the buoys, $\mathbf{x} = [\bar{x}_2, \bar{x}_3, \ldots, \bar{x}_N, \bar{y}_2, \bar{y}_3, \ldots, \bar{y}_N]$, where the pair $(\bar{x}_i, \bar{y}_i)$ represents the coordinates of the $i$th WEC. Therefore, $\mathbf{x}$ is taken as the input of the GP models. For the model output, we are interested in the wave excitation force vector $\mathbf{F}$, added mass coefficient matrix $\mathbf{a}$, and added damping coefficient matrix $\mathbf{b}$ described in Section 2. In this paper, we build separate GP models to predict the elements of $\mathbf{F}$, $\mathbf{a}$, and $\mathbf{b}$ (i.e., $F^{(p)}$, $a^{(pq)}$, and $b^{(pq)}$, where $p, q = 1, \ldots, N$), and the reason will be discussed later. Note that the wave excitation forces are complex values, and we separately predict the real and imaginary parts. With the model input and output selected, corresponding GP models can be constructed.

However, the standard way of building GP model faces significant challenges. Directly taking coordinates as inputs cannot incorporate our prior knowledge about the input-output relationship, such as the physical constraints including invariance, symmetry, and additivity (will be discussed in detail later), into the surrogate modeling. These features can only be learned by a large number of training data, but a lot of times we cannot obtain so many training data due to the high cost of running the numerical model (e.g., the MS solver). As a result, the prediction accuracy and generalization ability of the GP model under a limited number of training data may be significantly reduced. This is especially the case for arrays with a large number of WECs, since the large input space typically requires more training data to obtain desired prediction accuracy. However, the computational time of calculating the hydrodynamic characteristics increases dramatically with the number of WECs, which means obtaining training data is more costly as well.

To address the challenges in constructing a GP model to predict the hydrodynamic characteristics, this paper proposes a physics-constrained GP model that explicitly embeds the available physical constraints into the surrogate modeling process and eliminates the need for preparing a large training data set. This section first summarizes the physical characteristics/constraints of the relationship between the WEC layout and the hydrodynamic characteristics of WECs. Then, for different hydrodynamic characteristics, different model inputs are selected so that the physical constraints can be encoded appropriately and conveniently. Finally, in order to provide "informative prior knowledge" to the GP models, a physics-constrained GP model through designing specific kernels is proposed.

#### *3.2.1. Physical constraints of hydrodynamic interaction model: invariance, symmetry, and additivity*

First, in many engineering problems, the interested system often exhibits invariance or symmetry features, meaning some transformations on the model input do not change the model output. For example, in a chemical environment, the interatomic potential of a molecule or crystal is permutation-invariant with

respect to the ordering of the atoms in the same species [26]. In general, such invariance and symmetry knowledge about a function $f(\mathbf{x})$ can be formulated as

$$f(\mathbf{x}) = f(g(\mathbf{x})) \quad \forall \mathbf{x} \in \mathcal{X} \quad \forall g \in G \tag{7}$$

where $g(\mathbf{x})$ is an operation/transformation on the input $\mathbf{x}$ that determines the invariance/symmetry, and $G$ represents a finite group of all possible such operations. Note that the function $f$ is also invariant to the compositions of the operations [27], and thus the group $G$ includes both the operations and their possible compositions.

In the hydrodynamic interaction problem, we also have some prior knowledge about the invariance and symmetry features that the hydrodynamic characteristics exhibit, and they are essentially derived based on the physical laws of the hydrodynamic interaction problem and based on the underlying principles of the numerical model (i.e., MS solver) for calculating the hydrodynamic interaction. For the WEC array with $N$ buoys shown in Figure 1(c) represented by $\mathbf{x} = [\bar{x}_2,\ \bar{x}_3,\ \ldots,\ \bar{x}_N,\ \bar{y}_2,\ \bar{y}_3,\ \ldots,\ \bar{y}_N]$, the physical constraints are summarized as below:

(1) The wave excitation force of the buoy $p$ (i.e., $\mathrm{Re}\big[F^{(p)}\big]$ and $\mathrm{Im}\big[F^{(p)}\big]$ where $p = 1 \ldots N$) is permutation-invariant to the ordering of the rest of the buoys in the array;

(2) The added mass and damping coefficient matrices (i.e., $\mathbf{a}$ and $\mathbf{b}$) are symmetric, which means the added mass and damping coefficients of buoy $p$ due to the heave oscillation of buoy $q$ are equal to the added mass and damping coefficients of buoy $q$ due to the heave oscillation of buoy $p$;

(3) The diagonal terms of added mass and damping coefficient matrices ($a^{(pp)}$ and $b^{(pp)}$) where $p = 1 \ldots N$, are permutation-invariant with respect to the ordering of the rest of the buoys in the array. The off-diagonal terms of the matrices ($a^{(pq)}$ and $b^{(pq)}$ where $p, q = 1 \ldots N$ and $p \neq q$), are permutation invariant with respect to the ordering of the rest of the buoys in the array (i.e., all the buoys in the array excluding buoy $p$ and buoy $q$ themselves);

(4) Since any layout of the WEC array can be transformed to a new one with incident wave angle $\beta$ equal to zero, under zero incident angle, the hydrodynamic characteristics of all the buoys stay the same when the layout is reflected with respect to the $x$-axis. This symmetry property is illustrated in Figure 2.

The invariance and symmetry information summarized above can be encoded mathematically through Eq. (7). For example, suppose the array has three buoys and the coordinate vector used to characterize the layout is $\mathbf{x} = [\bar{x}_2,\ \bar{x}_3,\ \bar{y}_2,\ \bar{y}_3]$. Then the operations for the wave excitation force of buoy 1 (i.e., $F^{(1)}$) can be expressed by

$$\begin{aligned} &g_1([\bar{x}_2,\ \bar{x}_3,\ \bar{y}_2,\ \bar{y}_3]) = [\bar{x}_2,\ \bar{x}_3,\ \bar{y}_2,\ \bar{y}_3], \quad g_2([\bar{x}_2,\ \bar{x}_3,\ \bar{y}_2,\ \bar{y}_3]) = [\bar{x}_3,\ \bar{x}_2,\ \bar{y}_3,\ \bar{y}_2] \\ &g_3([\bar{x}_2,\ \bar{x}_3,\ \bar{y}_2,\ \bar{y}_3]) = [\bar{x}_2,\ \bar{x}_3, -\bar{y}_2, -\bar{y}_3], \quad g_4([\bar{x}_2,\ \bar{x}_3,\ \bar{y}_2,\ \bar{y}_3]) = [\bar{x}_3,\ \bar{x}_2, -\bar{y}_3, -\bar{y}_2] \end{aligned} \tag{8}$$

where $g_1(\cdot)$ represents "no operation", $g_2(\cdot)$ represents swapping WEC 2 and 3, $g_3(\cdot)$ represents reflecting the

WEC layout with respect to the $x$-axis, and $g_4(\cdot)$ represents swapping WEC 2 and 3 first and then reflecting the entire layout with respect to the $x$-axis.

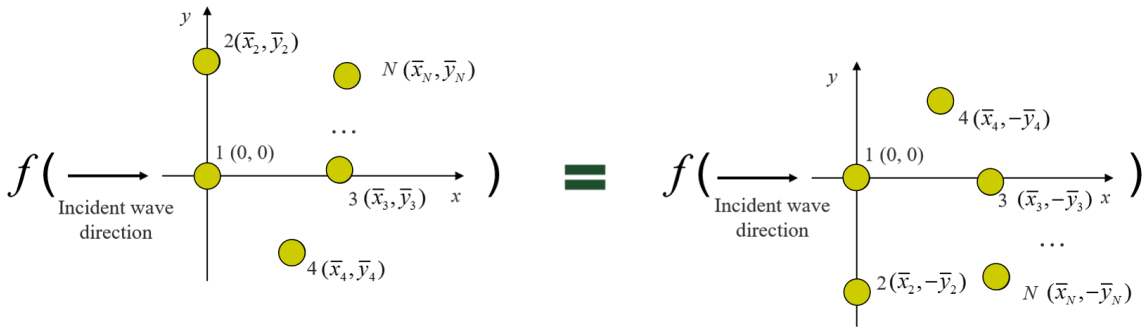


Figure 2: Illustration of symmetry property of hydrodynamic characteristics.

Second, the hydrodynamic interaction problem involves wave interactions between multiple floating bodies and resembles the classical many-body interaction problem in many fields such as quantum mechanics and molecular dynamics [28, 29]. As informed in the work by Zhang et al. [14] (which studied surrogate modeling of hydrodynamic forces between multiple floating bodies), the model output of this problem (i.e., hydrodynamic characteristics) can be decomposed into contributions from subsets of the buoys, represented by many-body terms (i.e., individual terms and interaction terms), and approximated by the series truncated at some finite orders. Mathematically, we formulate such decomposition as

$$y(\mathbf{x}) = \sum_{2\le i\le N} y_i(\mathbf{x}_i) + \sum_{2\le i<j\le N} y_{ij}(\mathbf{x}_i,\mathbf{x}_j) + \cdots + \sum_{2\le i<j<\cdots<l\le N} y_{ij\ldots l}(\mathbf{x}_i,\mathbf{x}_j,\ldots,\mathbf{x}_l) + \cdots \tag{9}$$

where $\mathbf{x}_i = (\bar{x}_i, \bar{y}_i)$ is the coordinate vector of the $i$th WEC. $y$ represents the quantity of interest such as any element of force vector $\mathbf{F}$, added mass coefficient matrix $\mathbf{a}$, or added damping coefficient matrix $\mathbf{b}$. $y_i$ denotes the response attributed to the $i$th buoy, $y_{ij}$ denotes the response attributed to the interaction between the $i$th and the $j$th buoys, and $y_{ij\ldots l}$ denotes the response attributed to the interaction between the $i$th, the $j$th, ..., and the $l$th buoys. The additivity feature is illustrated in Figure 3.

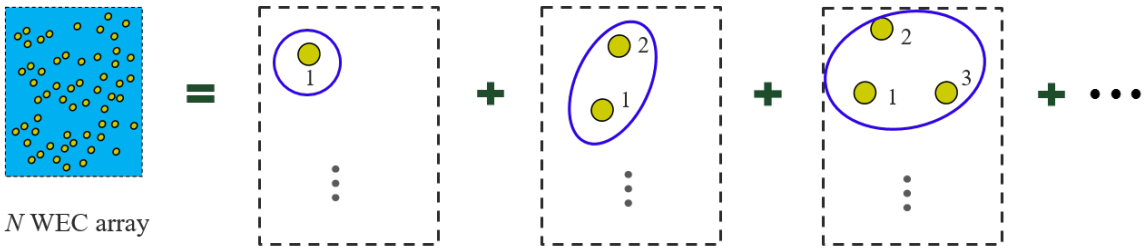


Figure 3: Illustration of decomposition of many-body systems (i.e., array of $N$ WECs).

The invariance, symmetry, and additivity features discussed above are deemed the physical constraints of

the hydrodynamic interaction model, and if this available prior knowledge can be incorporated when the GP models are constructed (e.g., encoded in the prior function assumed for the GP model), the required number of training data to reach good prediction accuracy is expected to be reduced. This reduction is especially important for building accurate GP models for arrays with a relatively large number of WECs, where the computational cost to obtain the training data is typically quite expensive.

*3.2.2. Selection of model input*

As summarized in the previous section, the permutation-invariance features of wave excitation force, added mass, and added damping coefficient may involve different buoys (i.e., corresponding to different model input); therefore, we separately predict these hydrodynamic characteristics. For different quantities of interest, we need to do some simple transformation (e.g., shift the coordinate system by some distances) on the original model input $\mathbf{x}$ so that the invariance and symmetry information can be appropriately and conveniently included in surrogate modeling.

First, we consider the model output $y = \mathrm{Re}\left[F^{(p)}\right]$, or $\mathrm{Im}\left[F^{(p)}\right]$, or $a^{(pp)}$, or $b^{(pp)}$, where $p = 1, \ldots, N$. In order to include the permutation invariance of the model outputs with respect to the ordering of all buoys except buoy $p$ in the GP model, we move the origin of the coordinate system to buoy $p$ and obtain a new coordinate vector, which will be used as the model input. Take the array with three WECs as an example: if we are interested in the added mass coefficient of WEC 2 due to its heave motion (i.e., $a^{(22)}$), we first augment the coordinate vector $\mathbf{x} = [\bar{x}_2,\ \bar{x}_3,\ \bar{y}_2,\ \bar{y}_3]$ to $\mathbf{x}_{aug} = [0,\ \bar{x}_2,\ \bar{x}_3,\ 0,\ \bar{y}_2,\ \bar{y}_3]$ and then shift the coordinate system so that the second buoy is the new origin. Finally, the new coordinate vector used to characterize the array layout becomes $\mathbf{x}_T = [-\bar{x}_2,\ \bar{x}_3,\ -\bar{y}_2,\ \bar{y}_3]$ (i.e., represented by the positions of WECs 1 and 3). It is noteworthy to point out that the added mass and damping coefficients are invariant with respect to any translational shift of the coordinate system, and thus the above transformation on the model input does not change the model outputs. However, any translational shift of the coordinate system along the wave propagation direction (i.e., $x$ direction when $\beta = 0$) can cause changes to the wave excitation forces. Therefore, in practice, when predicting the wave excitation force of buoy $p$ where $p = 2, \ldots, N$, we select the original coordinate vector as the model input (i.e., $\mathbf{x}_T = \mathbf{x}$), and release the constraint on the permutation invariance (switching the ordering of buoys except buoy 1 and buoy $p$ does not change $F^{(p)}$).

Second, for the off-diagonal terms of added mass and damping coefficient matrices ($y = a^{(pq)}$ or $b^{(pq)}$, where $p, q = 1, \ldots, N$ and $p \neq q$), we also move the origin of the coordinate system to the body $p$ so that the permutation invariance with respect to the ordering of the buoys except buoy $p$ and buoy $q$ can be considered conveniently, and the transformed coordinate vector is also represented by $\mathbf{x}_T$. It should be noted that in this case we also release the constraint on the permutation invariance since switching the ordering of buoy $p$ and buoy $q$ does not change the value of $a^{(pq)}$ or $b^{(pq)}$.

*3.2.3. Physics-constrained GP model through kernel design*

In order to incorporate the physical constraints of the hydrodynamic interaction model (i.e., invariance, symmetry, and additivity) to the GP model, we propose a physics-constrained GP model through kernel design. As discussed in Section 3.1, kernel is an crucial ingredient of a GP model. Consider two input locations $\mathbf{x}$, $\mathbf{x}'$ and their corresponding model outputs $y(\mathbf{x})$, $y(\mathbf{x}')$, a kernel $k(\cdot)$ is used to measure the covariance (representing similarity or distance) between the model outputs at two input locations, written as

$$\mathrm{Cov}(y(\mathbf{x}), y(\mathbf{x}')) = k(\mathbf{x}, \mathbf{x}') \tag{10}$$

The kernel function in the GP model typically assumes that the covariance between model outputs at two input locations decays smoothly as the distance between these inputs increases [30, 10], i.e., if $\mathbf{x}$ are close to $\mathbf{x}'$, $y(\mathbf{x})$ will be similar to $y(\mathbf{x}')$. Such kernel functions lie in the category of stationary kernel function, which is a function of the distance between inputs $\mathbf{x} - \mathbf{x}'$. Commonly used stationary kernel functions include the squared exponential kernel (shown in Eq. (11)), Matérn kernels (shown in Eq. (12)$\sim$(13)), rational quadratic kernel (shown in Eq. (14)), and more details about these kernel functions can be found in [10].

- Squared exponential kernel

$$k(\mathbf{x}, \mathbf{x}') = \sigma^2 \prod_{i=1}^{n_x} \exp\left(-\frac{|x_i - x_i'|^2}{2\theta_i^2}\right) \tag{11}$$

- Matérn 5/2 kernel

$$k(\mathbf{x}, \mathbf{x}') = \sigma^2 \prod_{i=1}^{n_x} \left(1 + \frac{\sqrt{5}|x_i - x_i'|}{\theta_i} + \frac{\sqrt{5}|x_i - x_i'|^2}{3\theta_i^2}\right) \exp\left(-\frac{\sqrt{5}|x_i - x_i'|}{\theta_i}\right) \tag{12}$$

- Matérn 3/2 kernel

$$k(\mathbf{x}, \mathbf{x}') = \sigma^2 \prod_{i=1}^{n_x} \left(1 + \frac{\sqrt{3}|x_i - x_i'|}{\theta_i}\right) \exp\left(-\frac{\sqrt{3}|x_i - x_i'|}{\theta_i}\right) \tag{13}$$

- Rational quadratic kernel

$$k(\mathbf{x}, \mathbf{x}') = \sigma^2 \prod_{i=1}^{n_x} \left(1 + \frac{|x_i - x_i'|^2}{2\alpha\theta_i^2}\right)^{-\alpha} \tag{14}$$

where $x_i$ and $x_i'$ are the $i$th component of the input $\mathbf{x}$ and $\mathbf{x}'$, respectively. Note that the distances between inputs are calculated in the Euclidean space in this study. A kernel function have several hyperparameters, which have significant influence on the established GP model. Take the squared exponential kernel in Eq. (11) as an example, $\sigma^2$ is the variance which tunes the amplitude of the model and $\boldsymbol{\theta} = [\theta_1, \ldots, \theta_{n_x}]$ are the length-scales which control the wiggliness of the model. We can also use the same $\theta$ for all components, and the corresponding kernel is the isotropic kernel. For the rational quadratic kernel, $\alpha$ is the scale mixture parameter.

In order to obtain the desired prediction performance, selecting an expressive valid kernel function is especially important since it determines the prior function assumed for the GP model. Therefore, here we

propose to impose the already known physical constraints into the kernel, and in this way a more "informative prior knowledge" can be provided for the GP model construction. In this section, an invariant kernel is first developed based on the invariance and symmetry information on the hydrodynamic interaction model and a base kernel (e.g., commonly used kernel functions). After that, an additive kernel is designed to incorporate the additive characteristics of the hydrodynamic interaction model and is then combined with the invariant kernel. The integrated kernel can explicitly consider the invariance, symmetry, and additivity features and be used to build GP models with high interpretability and generalization ability to predict the hydrodynamic characteristics for arrays with different layouts.

First, in order to build a GP model that is invariant under the operations in $G$ (see Eq. (7)), the proposed invariant kernel function should be invariant under the same operations. Ginsbourger et al. [31] have shown that a GP model is invariant to the operations in the group $G$ if and only if $k$ is argument-wise invariant to these operations, meaning it satisfys the following property:

$$k(\mathbf{x}_T, \mathbf{x}'_T) = k(g(\mathbf{x}_T), g'(\mathbf{x}'_T)) \quad \forall \mathbf{x}_T, \mathbf{x}'_T \in \mathcal{X} \quad \forall g, g' \in G \tag{15}$$

This kernel will be established by double-summing a base kernel defined earlier (e.g., one of the commonly used kernels defined in Eq. (11)$\sim$(14)) over the orbits of the inputs, where the orbit of $\mathbf{x}_T$ is the set of all transformed inputs obtained by applying each possible operation in $G$ to $\mathbf{x}_T$, and can be represented by the set $\mathcal{A}(\mathbf{x}_T) = \{g(\mathbf{x}_T); g \in G\}$. Formally, the invariant kernel is given by

$$k(\mathbf{x}_T, \mathbf{x}'_T) = \sum_{\mathbf{x}_T \in \mathcal{A}(\mathbf{x}_T)} \sum_{\mathbf{x}'_T \in \mathcal{A}(\mathbf{x}'_T)} k_{base}(\mathbf{x}_T, \mathbf{x}'_T) \tag{16}$$

In this application, the operations in the group $G$ include permutation of the WECs (i.e., switching the orders), symmetric mapping with respect to the $x$-axis and their composition. To this end, the GP model constructed using the invariant kernel function $k$ will be capable of integrating our prior knowledge (i.e., invariance and symmetry information) about the physical characteristics of the problem.

Second, we embed our knowledge about the additive features of the hydrodynamic characteristics. To build a GP model with the additive features, a new class of kernel is defined. It has been proved that the additivity of the GP model can be expressed by the additivity of the corresponding kernels [32]. Therefore, the GP model in our problem is specified by a kernel that can be decomposed into a series of subkernels with each sub-kernel corresponding to the contribution from the interaction between subsets of WECs with different numbers of WECs. Such a kernel is defined as the additive kernel, and it has the following expression:

$$\begin{aligned} k_{add}(\mathbf{x}_T, \mathbf{x}'_T) = \sigma_1^2 \sum_{2 \le i_1 \le N} k_{i1}(\mathbf{x}_{T,i_1}, \mathbf{x}'_{T,i_1}) + \sigma_2^2 \sum_{2 \le i_1 < i_2 \le N} k_{i_1}(\mathbf{x}_{T,i_1}, \mathbf{x}'_{T,i_1}) k_{i_2}(\mathbf{x}_{T,i_2}, \mathbf{x}'_{T,i_2}) + \cdots \\ + \sigma_t^2 \sum_{2 \le i_1 < i_2 \le \cdots \le i_t \le N} \prod_{d=1}^{t} k_{id}(\mathbf{x}_{T,i_d}, \mathbf{x}'_{T,i_d}) + \cdots \end{aligned} \tag{17}$$

where $\{k_{id}(\mathbf{x}_{T,id}, \mathbf{x}'_{T,id}), d = 2, 3, \ldots, N\}$ is a base kernel operating on two dimensions of the input $\mathbf{x}_T$ and $\mathbf{x}'_T$ (i.e., the transformed coordinates of the $d$th WEC), and $\sigma_t^2$ is the variance assigned to the $t$th interaction term. In order to specify the additive kernel, one needs to select a base kernel function first, and then optimize the hyperparameters, including the length scale of the base kernel and the variance $\sigma_t^2$ in each order based on the given training data. Note that different variance values can be specified for each sub-kernel of the additive kernel which also helps the GP model control the variance assigned to each order of interaction of the input.

Finally, the additive kernel in Eq. (17) is combined with the invariant kernel in Eq. (16), and more specifically, the base kernel of the invariant kernel takes the additive kernel:

$$k(\mathbf{x}_T, \mathbf{x}'_T) = \sum_{\mathbf{x}_T \in \mathcal{A}(\mathbf{x}_T)} \sum_{\mathbf{x}'_T \in \mathcal{A}(\mathbf{x}'_T)} k_{add}(\mathbf{x}_T, \mathbf{x}'_T) \tag{18}$$

To better explain how the proposed physics-constrained kernel works, Figure 4 illustrates the evaluation process of the proposed kernel for any 3-WEC array. The integrated kernel is then used to develop GP models for the hydrodynamic characteristics. It is noteworthy to point out that the computational cost of evaluating the proposed kernel in Eq. (18) is expensive when the dimension of the input is large. However, if the many-body system converges fast, we can truncate the interaction series to a low order, which will help reduce the computational effort in building the GP model. In our problem, the decomposition in Eq. (9) is expected to converge fast (i.e., the first several orders of interaction contribute much to the response) based on the justification given in [14]. That is, the MS method provides an exact solution for the hydrodynamic characteristics by summing the infinite scattering order, whose superior convergence rate has been confirmed, and many-body expansion has a faster convergence speed than the MS method. This principle also applies to the GP model with a similar additive structure. Therefore, in this application, it is expected that only the first few orders of interactions are important for modeling the hydrodynamic characteristics. This assumption naturally suggests that, when the computational resources are limited, one can limit the maximum considered order of interaction for the additive kernel without significantly impacting the prediction accuracy. In the end, the computational cost of evaluating Eq. (18) can be significantly reduced.

### *3.3. Overall algorithm*

The overall algorithm of the proposed physics-constrained GP model for predicting hydrodynamic characteristics of WEC arrays is illustrated in Algorithm 1, which shows the key steps. In the algorithm, the output of the GP model is scalar meaning a separate GP model is built for each element of $\mathbf{F}$, $\mathbf{a}$ and $\mathbf{b}$. Therefore, for an array of $N$ WECs, we need to train $2N + 2(N^2 + N)/2 = N^2 + 3N$ GP models in total. However, in practice, we can train a model to predict some elements together if they depend on the same model input (e.g., $\mathrm{Re}\big[F^{(11)}\big]$, $\mathrm{Im}\big[F^{(11)}\big]$, $a^{(11)}$, and $b^{(11)}$). In this way, the number of GP models needed to be trained is reduced to $N + N - 1 + (N^2 - N)/2 = (N^2 + 3N)/2 - 1$ at most, which is less than half of the original required number of GP models.

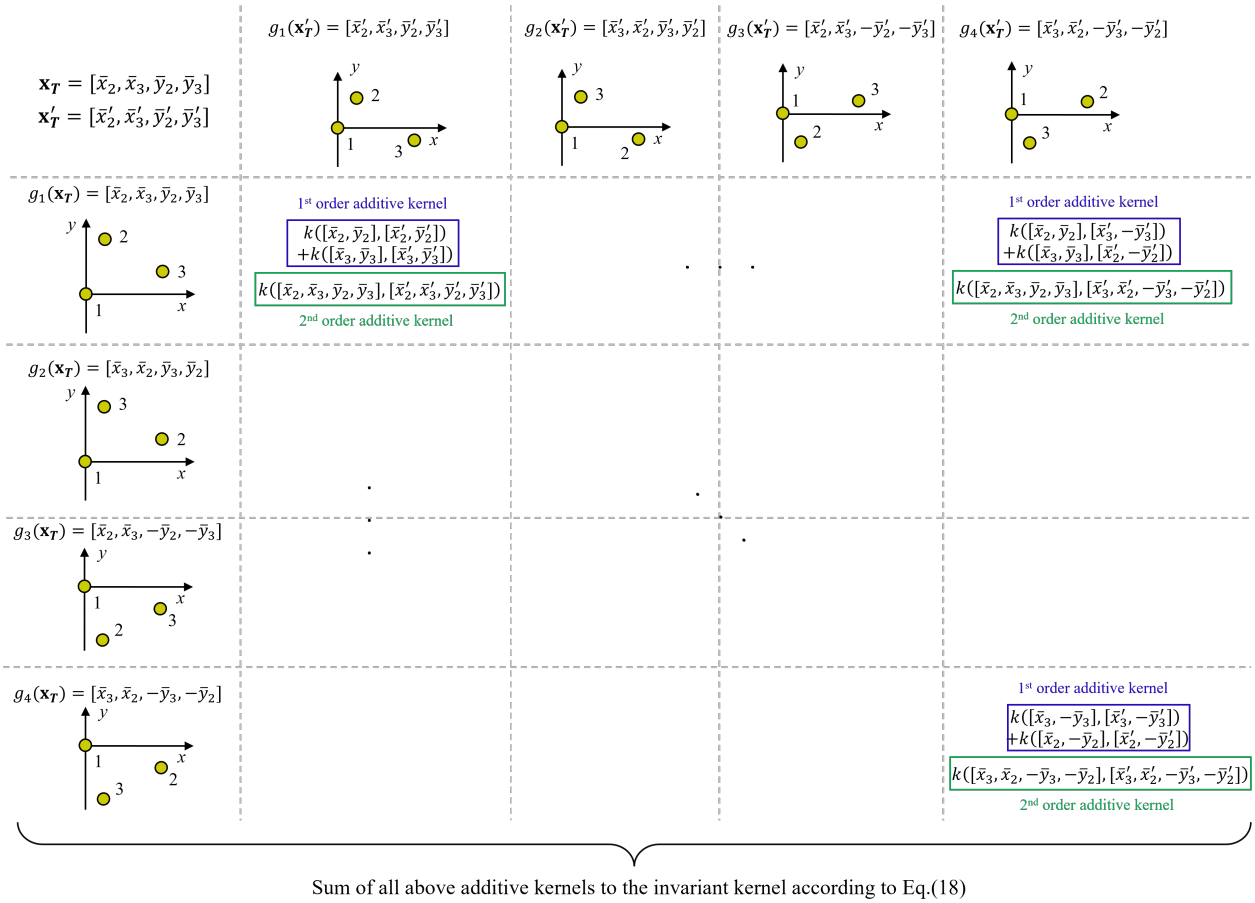


Figure 4: Illustration of the evaluation process of the physics-constrained kernel between any two 3-WEC arrays represented by $\mathbf{x}_T$ and $\mathbf{x}'_T$.

For any new WEC array shown in Fig 1(c), we first transform the layout to a new one with incident angle $\beta = 0$, and the corresponding coordinate vector is denoted $\mathbf{x}_0$. For any model output of interest, we then transform $\mathbf{x}_0$ to appropriate $\mathbf{x}_{T,0}$ by simply moving the coordinate system according to Section 3.2.2. Then the trained GP models can be used to directly predict the elements of the hydrodynamic characteristics for the considered wave frequency $\omega$. Finally, the elements are assembled to establish the corresponding vector $\mathbf{F}$ or matrices $\mathbf{a}$ and $\mathbf{b}$.

## 4. Illustrative Example

To demonstrate the performance of the proposed algorithm, it is applied to predict hydrodynamic characteristics of WECs in an array. The array is in a rectangular domain with 127.5 m along the $x$-axis and 255 m along the $y$-axis, and the water depth is 60 m. The buoys are identical cylinders oscillating in heave direction only. The radius for each buoy is $r_b = 3$ meters and its mass is $m_b = 1.8\text{e}5$ kg, corresponding to a draft of $D_r = 6.37$ m and natural period of oscillation of 5.06 s. The considered wave frequency is 0.6 rad/s and it corresponds to a wave period equal to 10 s which has a high occurrence probability. To investigate

**Algorithm 1** The proposed physics-constrained GP model

Step 1: Represent layout of an array with $N$ WECs (Figure 1(c) with $\beta = 0$) using a coordinate vector $\mathbf{x} = [\bar{x}_2, \bar{x}_3, \ldots, \bar{x}_N, \bar{y}_2, \bar{y}_3, \ldots, \bar{y}_N]$

Step 2: Generate input matrix $\mathbf{X} = \{\mathbf{x}^h; h = 1, \ldots, n\}$ (i.e., using Latin Hypercube Sampling (LHS)), and run expensive model (i.e., MS solver) for each $\mathbf{x}^h$ to obtain hydrodynamic characteristics ($\mathbf{Y} = \mathbf{F}^h, \mathbf{a}^h,$ or $\mathbf{b}^h$) at a specific wave frequency $w$

Step 3: Obtain the model input matrix $\mathbf{X}_T = \{\mathbf{x}_T^h; h = 1, \ldots, n\}$ by transforming each model input $\mathbf{x}$ to $\mathbf{x}_T$ according to Section 3.2.2

Step 4: Design kernel to encode permutation invariance, symmetry, and additivity properties according to Section 3.2.3

Step 5: Based on input-output pairs $\{\mathbf{X}_T, \mathbf{Y}\}$, develop a physics-constrained Gaussian process model

the impact of the wave frequency on the model construction, wave frequencies between 0.3 rad/s and 1.3 rad/s (i.e., wave periodic between 4.8 s and 20.9 s) are also considered. The corresponding wave number $k$ varies from 0.0136 1/m to 0.1723 1/m. The incident angle $\beta$ is selected as 0 in this example, but generally it can take any value. In order to investigate the scalability of the proposed algorithm, it is applied to arrays with different numbers of WECs, and here $N$ in the range of 3 to 30 is considered.

### *4.1. Implementation details*

To establish the training data set, $n$ inputs are generated by LHS and the corresponding outputs are calculated by the hydrodynamic interaction model using the MS approach. For the MS solver, the order of interaction is set as 5, whereas the eigenfunction series are truncated at 5 and 40 for the main fluid and the fluid below the cylinder, respectively, to ensure adequate accuracy. These values are selected through a convergence study of the model. More details can be found in the Appendix. In the proposed physics-constrained GP model, the kernel is the invariant kernel in Eq. (16) taking the additive kernel in Eq. (17) as base kernel, and for the base kernel of additive kernel, we select the commonly used Matern kernel with $\nu = 5/2$. Since decomposition in Eq. (9) is expected to converge fast, we infer that only the first several orders of interaction in Eq. (17) contribute much to the model response. To validate this assumption with the currently available computational resource, we used the additive kernel with full orders of interaction for the WEC arrays with 3 buoys and 4 buoys, and the contribution from each order is characterized by the assigned variance $\sigma_t^2$, where $t = 1, 2$ for the 3-WEC array and $t = 1, 2, 3$ for the 4-WEC array. After optimization of the hyperparameters, the results for all the diffraction- and radiation-related hydrodynamic characteristics show that for the 3-WEC array, $\sigma_1^2 \approx 1$ while $\sigma_2^2 \approx 0$. Similarly, for the 4-WEC array, $\sigma_1^2 \approx 1$ while $\sigma_2^2, \sigma_3^2 \approx 0$. Both cases indicate that only the first order of interaction between the buoys contributes most to the hydrodynamic coefficients predicted by the physics-constrained GP model. Therefore, for all the other cases, we limit the maximum considered order of interaction for the additive kernel to the first order and assume that this implementation will not significantly impacting the prediction accuracy. This significantly

reduces the computational effort in evaluating the kernel functions. For comparison purposes, a standard GP model, which is the same as the proposed model but uses the standard base kernel, is constructed to predict the same output. For the kernels in the proposed GP model and the standard GP model, we use the same length-scale value for all input dimensions. The reason for this selection here is that the computational effort to optimize a single length scale is typically much less than the effort to optimize multiple length scales, especially when the input dimensionality is high. More importantly, in this example using the same length scale for all the input dimensions can already inform an accurate Gaussian process model.

To assess the accuracy of the GP models in predicting the hydrodynamic characteristics, validation metrics are calculated over a testing set for each case. The test size is set as $n_t = 1000$, and the testing data are also generated by LHS. Figure 5 shows the statistics of the minimum, maximum, and average separation distance between WECs in an array calculated for the 1000 testing data. Here the coefficient of determination, $R^2$, is used as the validation metric,

$$R^2 = 1 - \frac{\sum_{i=1}^{n_t}(y^i - \hat{y}^i)^2}{\sum_{i=1}^{n_t}(y^i - \sum_{i=1}^{n_t} y^i/n_t)^2} \tag{19}$$

where $\hat{y}^i$ is the prediction from the established GP model for the $i$th data in the testing set. Large $R^2$ values (e.g., closer to 1) indicate that the trained model has good accuracy.

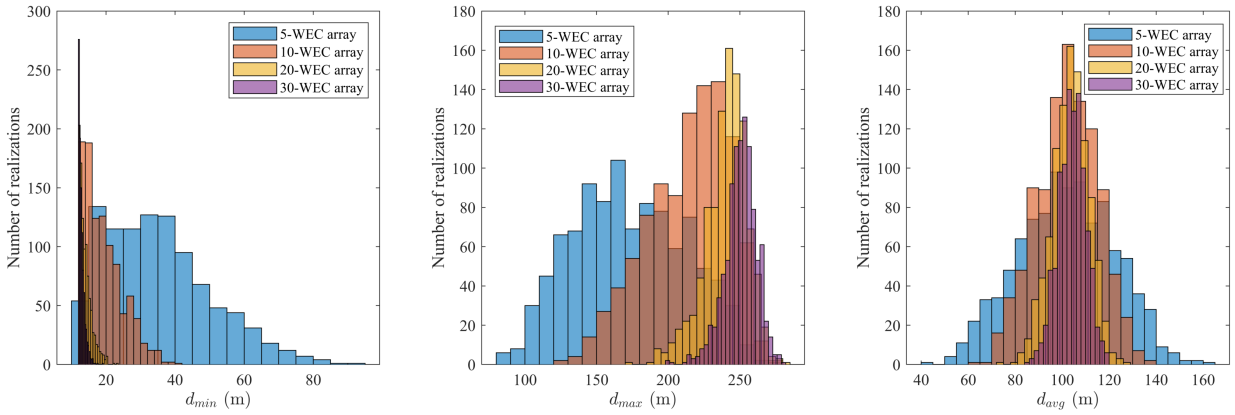


Figure 5: Statistics of the minimum ($d_{min}$), maximum ($d_{max}$), and average ($d_{avg}$) separation distance between WECs in an array for 1000 testing data.

### *4.2. Selection of training size and prediction accuracy*

To investigate the prediction accuracy of the proposed physics-constrained GP model, we calculate the coefficient of determination $R^2$ for all cases (i.e., arrays with different numbers of WECs). Due to space limitation, we only list the results for arrays of 3, 5, 8, 10, 20, and 30 WECs, while the results for other cases show a similar pattern. The prediction accuracy metrics are calculated separately for different elements of the hydrodynamic characteristic matrices $\mathbf{F}$, $\mathbf{a}$, and $\mathbf{b}$. For illustrative purposes, the elements are classified into four groups: (1) real and imaginary parts of $F^{(1)}$, (2) real and imaginary parts of $F^{(p)}$ where $p = 2, \ldots, N$,

(3) $a^{(pp)}$ and $b^{(pp)}$ where $p = 1, \ldots, N$, and (4) $a^{(pq)}$ and $b^{(pq)}$ where $p, q = 1, \ldots, N$ and $p \neq q$. The reason for such classification is that the prediction accuracies for the real and imaginary parts of $\mathbf{F}$ are close, and also the prediction accuracies for $\mathbf{a}$ and $\mathbf{b}$ are close. Additionally, when modeling $F^{(1)}$, $a^{(pp)}$, and $b^{(pp)}$, the strict invariance information is incorporated while only partial invariance information is considered when modeling $F^{(p)}$, $a^{(pq)}$, and $b^{(pq)}$. For each group, the mean of the accuracy metrics (i.e., $R^2$) is calculated, and to show the spread of prediction accuracy between different elements within a group, the minimum and maximum of the accuracy metrics are also calculated.

When constructing the physics-constrained GP model to replace the computationally expensive MS solver, it is desirable to use a small number of training data $n$, while maintaining the good prediction accuracy of the surrogate model. In order to select an appropriate $n$, we investigate how the model prediction accuracy changes over different $n$. Figure 6 shows the variation of the mean $R^2$ values against $n$ for arrays with different numbers (i.e., 5, 10, 20, and 30) of WECs when the wave frequency, $\omega$, is 0.6 rad/s. As expected, the mean $R^2$ increases when the training size increases. This is true for arrays with different WECs and for the different hydrodynamic characteristics. For the diffraction-related characteristics, the prediction accuracy is already superior (i.e., the mean $R^2$ values are larger than 0.98) when $n$ reaches 40 and has only small improvement when further increasing $n$. However, for the radiation-related characteristics, more training data are required to reach the targeted mean $R^2$ values (i.e., 0.98). The reasons for this is that the radiation-related characteristics show stronger nonlinearity with respect to the model input than the diffraction-related characteristics. Note that for a specific WEC array, different elements of the hydrodynamic coefficients come from one evaluation of the MS solver, and thus the same number $n$ should be selected for different hydrodynamic coefficients. As a result, the number of training data $n$ for 3-, 5-, 8-, 10, 20-, and 30-WEC arrays is selected as 100, 120, 120, 120, 160, and 180, respectively.

To further compare the prediction performance of the algorithm using a selected number of training data between different WEC arrays, we show the mean, minimum, and maximum of the prediction metrics in Table 1. For diffraction-related characteristics (i.e., elements of $\mathbf{F}$), as can be observed from the table, the $R^2$ for all cases are over 0.90, which reveals excellent prediction accuracy of the proposed physics-constrained GP model. In each case, by comparing the mean, minimum, and maximum of $R^2$ within a group of the hydrodynamic characteristics, we can find that the values are very close, which means there is little variation in the prediction accuracy for different elements of $\mathbf{F}$. For radiation-related characteristics (i.e., elements of $\mathbf{a}$ and $\mathbf{b}$), very good prediction accuracy can also be obtained, but the mean, minimum, and maximum values of $R^2$ for radiation-related hydrodynamic characteristics are relatively different. This indicates that the prediction accuracy for different elements of $a^{(pp)}/b^{(pp)}$ and $a^{(pq)}/b^{(pq)}$ show relatively large variability. Additionally, almost all the hydrodynamic characteristics experience a drop in the prediction accuracy as the number of WECs in the array increases, although the number of training data are also increased. This is expected since the dimensionality of the model input is proportional to the number of WECs in the array, and higher-dimensional input space requires more training data to inform an accurate GP model.

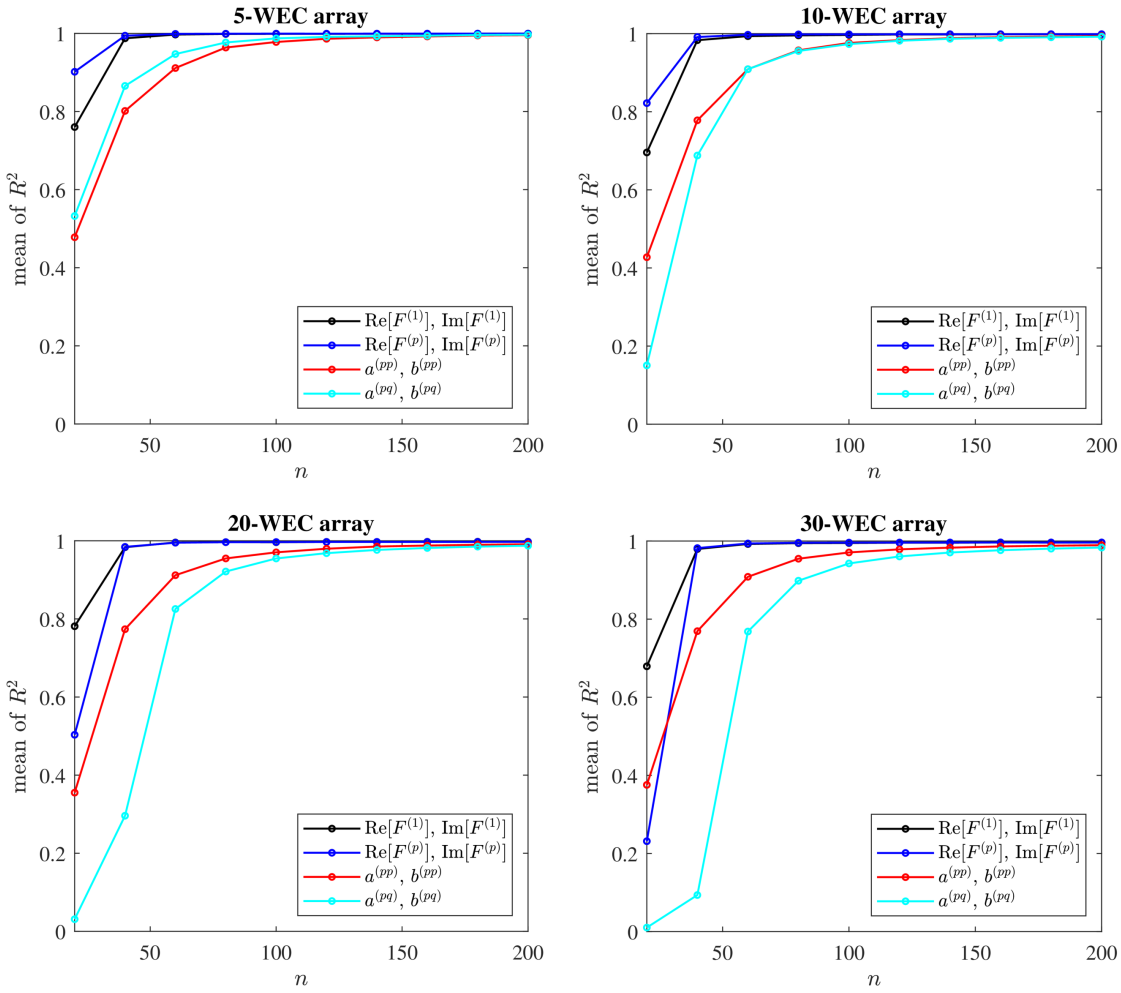


Figure 6: Variation of the mean of $R^2$ against the number of training data $n$ for arrays with different numbers of WECs (shown for the case when the wave frequency $\omega = 0.6$ rad/s).

### *4.3. Impact of wave frequency*

The prediction accuracy of the established surrogate model may be significantly affected by the wave frequency of interest. To investigate the impact of the wave frequency on the physics-constrained GP model, Figure 7 shows the variation of the mean $R^2$ values against wave frequency $\omega$ for all the hydrodynamic coefficients of arrays with different numbers of WECs. For comparison purposes, the physics-constrained GP models are developed for different wave frequencies with the same number of training data $n$, and $n$ is still selected as 120, 120, 160, and 180 for 5-, 10-, 20-, and 30-WEC arrays, respectively. The considered wave frequencies are between 0.3 rad/s and 1.3 rad/s, and since these two bounds have very low occurrence probability for most deployment locations, they can serve as good bounding cases to check the impact of the wave frequency on the prediction accuracy. It is noteworthy to point out that in this section the physics-constrained GP model is established for the multi-dimensional outputs consisting of the hydrodynamic coefficients under all the considered wave frequencies. As can be observed the figure, the prediction accuracy

| # of WECs | $\mathrm{Re}[F^{(1)}](\mathrm{Im}[F^{(1)}])$ | | | $\mathrm{Re}[F^{(p)}](\mathrm{Im}[F^{(p)}])$ | | |
|---|---|---|---|---|---|---|
| | mean | min | max | mean | min | max |
| 3 | 0.9989(0.9976) | 0.9989(0.9976) | 0.9989(0.9976) | 0.9997(0.9997) | 0.9996(0.9997) | 0.9997(0.9997) |
| 5 | 0.9989(0.9988) | 0.9989(0.9988) | 0.9989(0.9988) | 0.9993(0.9992) | 0.9991(0.9991) | 0.9994(0.9993) |
| 8 | 0.9982(0.9985) | 0.9982(0.9985) | 0.9982(0.9985) | 0.9988(0.9989) | 0.9986(0.9985) | 0.9992(0.9992) |
| 10 | 0.9980(0.9976) | 0.9980(0.9976) | 0.9980(0.9976) | 0.9985(0.9984) | 0.9982(0.9981) | 0.9988(0.9987) |
| 20 | 0.9971(0.9978) | 0.9971(0.9978) | 0.9971(0.9978) | 0.9971(0.9972) | 0.9961(0.9963) | 0.9976(0.9978) |
| 30 | 0.9967(0.9958) | 0.9967(0.9958) | 0.9967(0.9958) | 0.9964(0.9962) | 0.9951(0.9944) | 0.9970(0.9968) |
| # of WECs | $a^{(pp)}(b^{(pp)})$ | | | $a^{(pq)}(b^{(pq)})$ | | |
| | mean | min | max | mean | min | max |
| 3 | 0.9940(0.9819) | 0.9934(0.9787) | 0.9946(0.9872) | 0.9901(0.9984) | 0.9856(0.9958) | 0.9951(0.9998) |
| 5 | 0.9936(0.9788) | 0.9913(0.9725) | 0.9981(0.9962) | 0.9848(0.9976) | 0.9715(0.9935) | 0.9972(0.9994) |
| 8 | 0.9935(0.9742) | 0.9908(0.9629) | 0.9977(0.9936) | 0.9734(0.9955) | 0.9538(0.9855) | 0.9963(0.9990) |
| 10 | 0.9931(0.9736) | 0.9885(0.9663) | 0.9978(0.9945) | 0.9690(0.9943) | 0.9241(0.9824) | 0.9949(0.9986) |
| 20 | 0.9938(0.9819) | 0.9913(0.9718) | 0.9969(0.9937) | 0.9692(0.9941) | 0.9452(0.9833) | 0.9949(0.9974) |
| 30 | 0.9933(0.9828) | 0.9901(0.9776) | 0.9960(0.9922) | 0.9678(0.9932) | 0.9378(0.9848) | 0.9939(0.9970) |

Table 1: Mean, minimum, and maximum of prediction accuracy metrics when $\omega = 0.6$ rad/s

when $\omega = 0.6$ rad/s degrades compared to the results presented in Section 4.2, obtained from training the physics-constrained GP model for the single wave frequency 0.6 rad/s. From the figure, we can also observe that when the wave frequency is relatively low (e.g., less than 0.8 rad/s), all the $R^2$ values are greater than 0.6 and the prediction for all hydrodynamic characteristics demonstrates a relatively good agreement with the ground truth values. However, as the wave frequency increases, it becomes more challenging to predict the hydrodynamic characteristics accurately, especially for the radiation-related coefficients. The reason behind this observation is that the wavelength decreases as the wave frequency becomes larger based on the dispersion relation, and thus there are more peaks/troughs in the hydrodynamic data as wave frequency increases (i.e., the model input-output relationship becomes more complex). To further illustrate the impact of the wavelength on the prediction accuracy, Figure 8 plots the variation of the same mean $R^2$ values against $k \times l_x$ as in Figure 7, where $l_x$ is the array length along the $x$-direction. As can be seen from the figure, the prediction accuracy drops when the wavelength reduces, and when the array length is larger than approximately 10 times the wavelength, most of the mean $R^2$ values become less than 0.6.

One straightforward way to improve the prediction performance for predicting the hydrodynamic characteristics under relatively high wave frequencies is to use more training data within the available computational budgets. To investigate this, the number of training data for 5-, 10-, 20-, and 30-WEC arrays is increased to 5 times the original number of training data, i.e., 600, 600, 800, and 900, respectively, and the corresponding results are shown in Figure 9. As can be observed from the figure, increasing the number of training data directly is effective in improving the prediction accuracy. For example the mean $R^2$ for element $b^{(pq)}$ in the 5-WEC array dramatically increases from 0.01 to 0.87 when $\omega = 1.3$ rad/s. However, one drawback of this method is that we need to trade off between accuracy and efficiency. Increasing prediction accuracy for

high wave frequency usually demands a larger number of training data, resulting in heavier computational efforts in obtaining the data and also higher cost in training the surrogate model. In addition, adding more training data may only lead to a small gain in improving the prediction performance when the number of WECs in the array is large (e.g., 20- and 30-WEC arrays). Despite this, the lower prediction accuracy for higher frequencies is less of a concern in this application since very high wave frequencies typically have a low occurrence probability for most deployment locations.

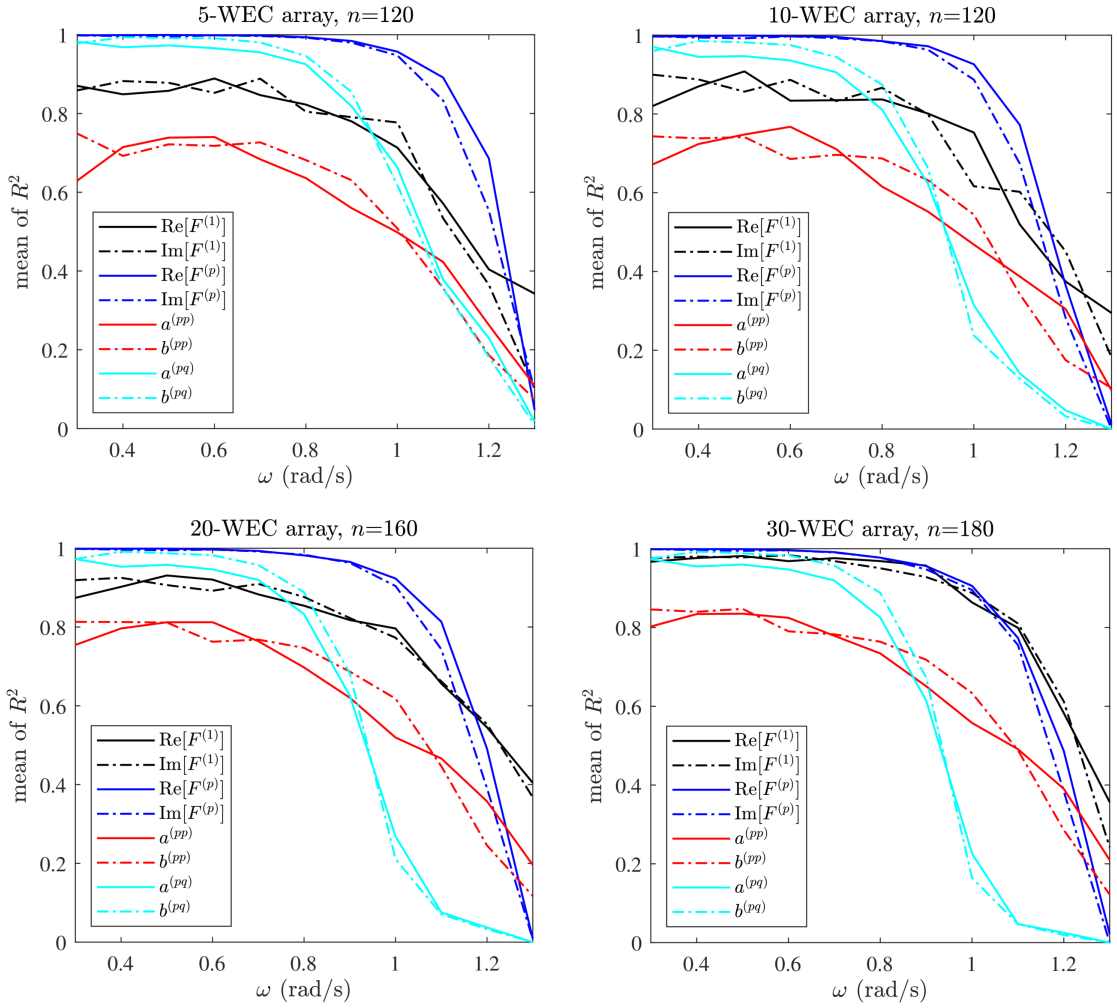


Figure 7: Prediction accuracy metrics against $\omega$ for arrays with different numbers of WECs.

### *4.4. Performance of physics-constrained kernel*

In this section, the performance of the kernel in the proposed physics-constrained GP model is investigated. For comparison purposes, a standard GP model with the Matern kernel with $\nu = 5/2$ is also constructed with the same training data set and validated using the same testing data as the physics-constrained GP model. For convenience, the kernel in the physics-constrained GP model and the standard GP model are referred to as the physics-constrained kernel and standard kernel, respectively, in this section.

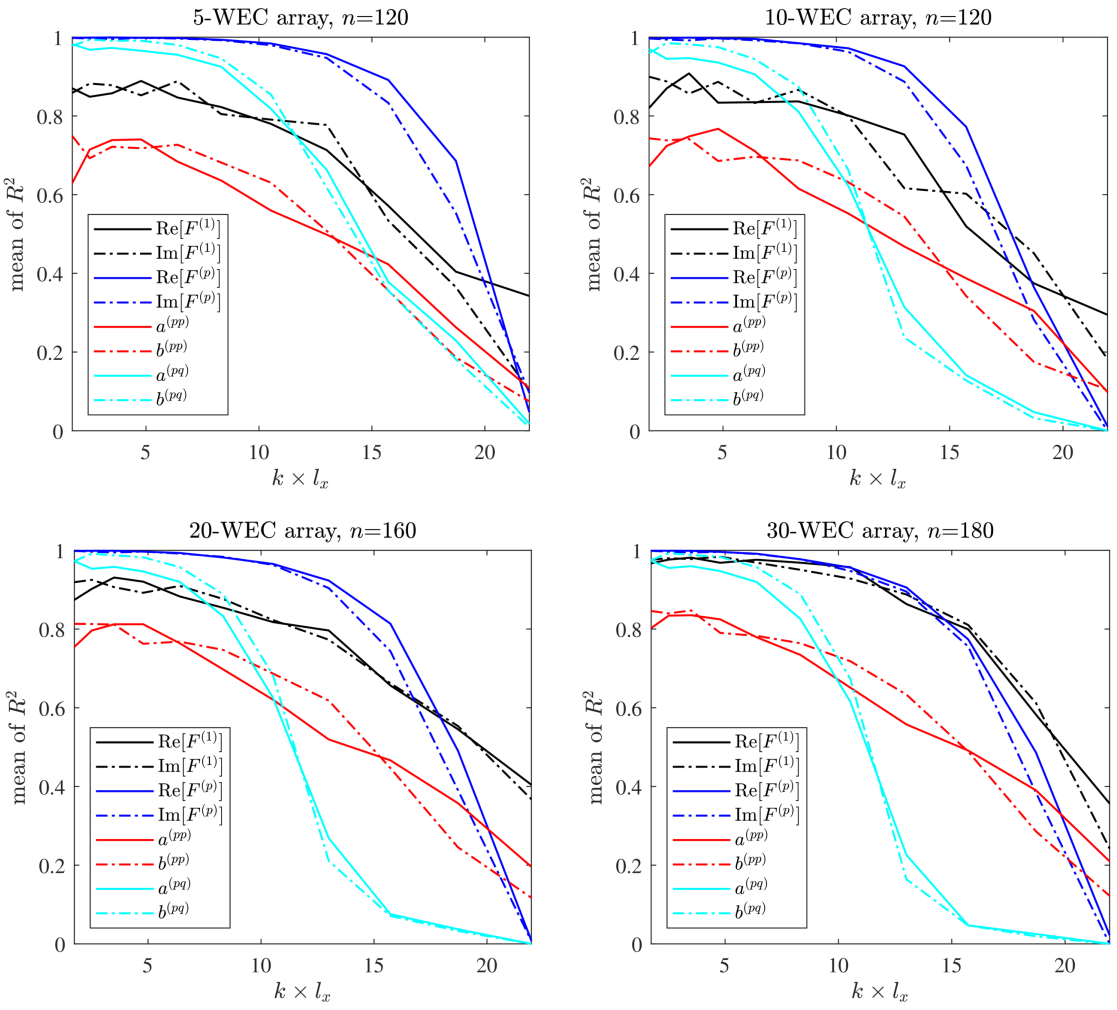


Figure 8: Prediction accuracy metrics against $k \times l_x$ for arrays with different numbers of WECs.

The main purpose of this section is to compare the performance of the physics-constrained GP model and the standard GP model, and thus the prediction accuracy for a single case is less of a concern here. Note that $\omega = 0.6$ rad/s is selected for demonstrating the results in this section.

The kernel function in a GP model specifies the covariance between the model response at two input locations, which implicitly describes the distance between two input locations. In order to visualize the capability of the physics-constrained kernel and the standard kernel in describing the similarity of the model response between the input points, Figure 10 illustrates the covariance function values evaluated at a data set $\mathbf{X}_T$ (i.e., covariance matrix $k(\mathbf{X}_T, \mathbf{X}_T)$). The data set contains four arrays of 3 WECs, characterized by $\mathbf{X}_T = \{\mathbf{x}_T^1, \mathbf{x}_T^2, \mathbf{x}_T^3, \mathbf{x}_T^4\}$, where $\mathbf{x}_T^1 = [123.5\ 93.2\ -59.2\ -116.4]$, $\mathbf{x}_T^2 = [93.2\ 123.5\ -116.4\ -59.2]$, $\mathbf{x}_T^3 = [123.5\ 93.2\ 59.2\ 116.4]$, and $\mathbf{x}_T^4 = [93.2\ 123.5\ 116.4\ 59.2]$. Among these four inputs, $\mathbf{x}_T^1$ is selected from the training set, and the other three are transformed from $\mathbf{x}_T^1$ based on the invariance and symmetry properties, as shown in Eq. (8). For illustration purposes, we added some Gaussian noises to the locations

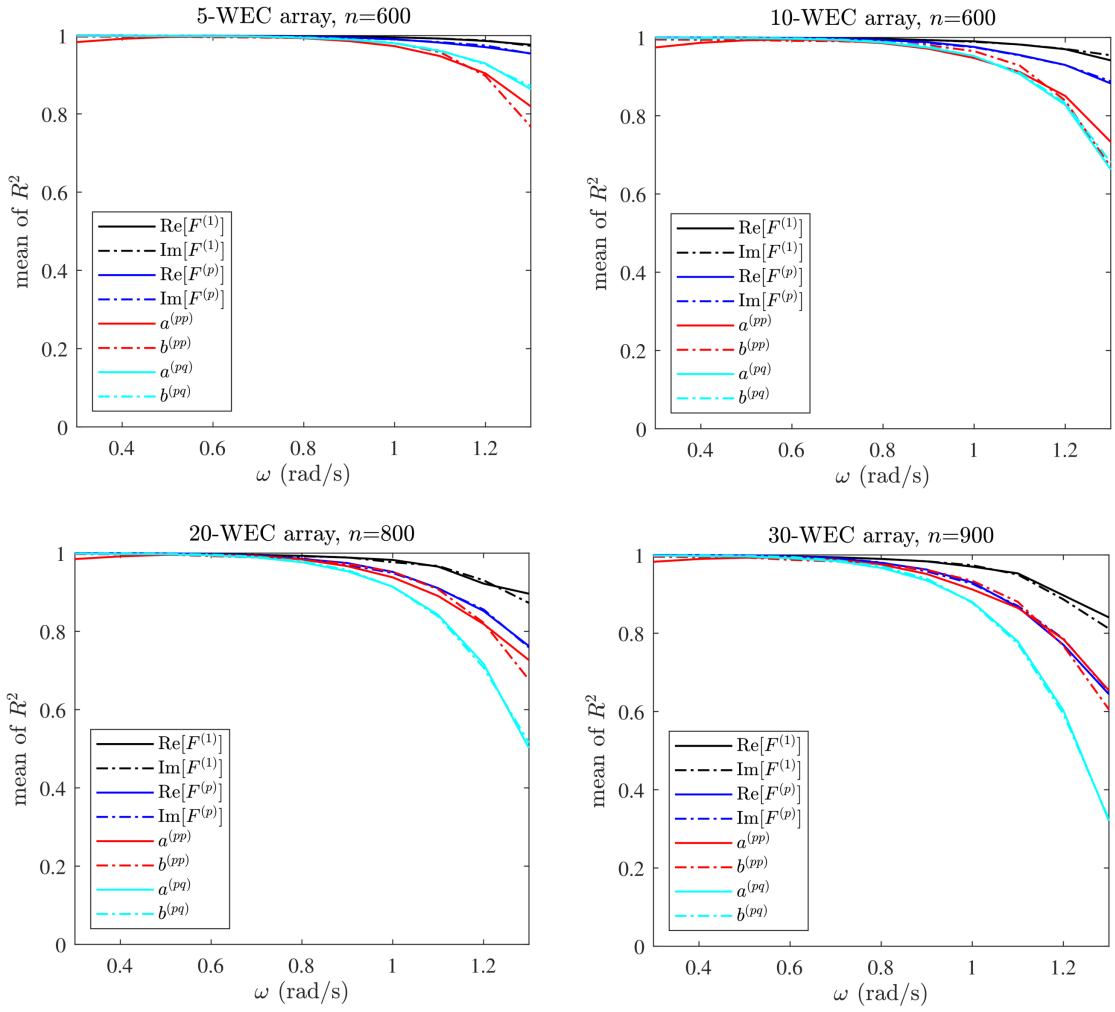


Figure 9: Prediction accuracy metrics against $\omega$ for arrays with different numbers of WECs when more training data are used.

of WECs. Note that here we focus on the physics-constrained kernel used for $F^{(1)}$, $a^{(pp)}$, and $b^{(pp)}$, which includes the complete permutation invariance and symmetry information available. In Figure 10, the value of each grid describes the covariance of the model response between two inputs, and for comparison, the values are normalized so that the diagonal terms of the covariance matrices are equal to one. As a result, the covariance values close to one means that two input points are close to each other and the their responses are also highly similar. As can be observed from the figure, the covariance calculated by the standard kernel between $\mathbf{x}_T^i$ and $\mathbf{x}_T^j$ $(i \neq j)$ is nearly zero, while the corresponding covariance calculated by the physics-constrained kernel is close to one. However, as we mentioned earlier, $\mathbf{x}_T^i$ and $\mathbf{x}_T^j$ $(i \neq j)$ should give us similar model responses due to the invariance and symmetry features of the input-output relationship. This indicates that the physics-constrained kernel has the capability of encoding the invariance and symmetry features into the GP model, while the standard kernel is not able to capture such properties.

To further demonstrate the performance of the physics-constrained GP model and the standard GP model

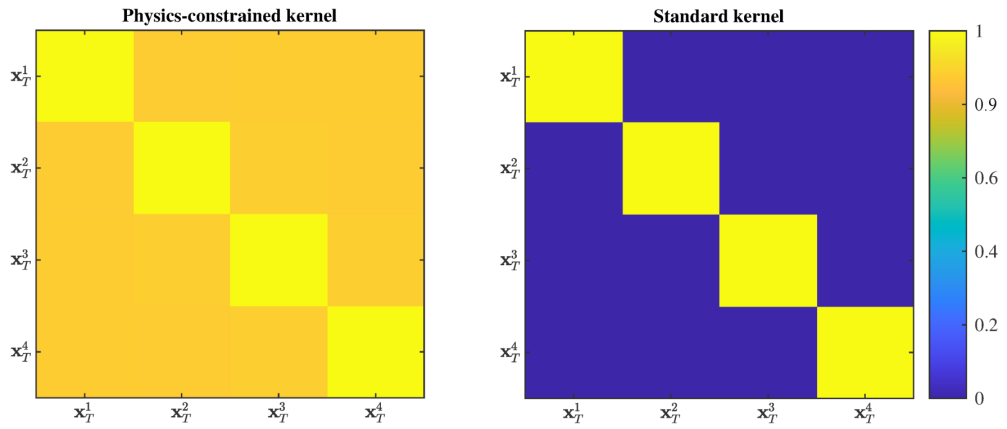


Figure 10: Covariance matrix calculated by physics-constrained kernel and standard kernel.

in recovering the ground truth input-output relationship, Figure 11 and Figure 12 show the model response $F^{(1)}$ calculated by the true function, predicted by the physics-constrained GP model and the standard GP model. In order to visualize the permutation invariance and symmetry features of the model response, we pick the array of 3 WECs and plot the contour map of $F^{(1)}$ with respect to $\mathbf{x}_{T,2}$ and $\mathbf{x}_{T,3}$, where $\mathbf{x}_{T,2}$ and $\mathbf{x}_{T,3}$ are the positions of the two WECs (i.e., WEC 2 and WEC 3) except the one at the origin of the coordinate system. First, Figure 11 shows the contour map of $F^{(1)}$ in terms of the positions of WEC 2 and WEC 3 characterized by some ID numbers. More specifically, the input domain is divided into a 5-by-9 grid, and the nodes of the grid are assigned a sequence of ID numbers. As a result, each ID number represents a position that WEC 2 and WEC 3 may take in the input domain, and thus in Figure 11 the horizontal and vertical axes correspond to the positions of WEC 2 and WEC 3, respectively. As can be observed from the figure, the true function of $F^{(1)}$ is symmetrical with respect to the diagonal line, which means switching the position of WEC 2 and WEC 3 does not change the model response. Note that the diagonal line in the figure is blank because the two buoys cannot be overlapped with each other physically. The physics-constrained GP model can correctly recover such permutation invariance feature since such feature has been entirely coded into the kernel, while the standard GP model fails to capture the permutation invariance. However, we can find some slight symmetry property with respect to the diagonal line predicted by the standard GP model, which might have been learned by the training data, and if more training data are used, it is expected that the constructed standard GP model might be able to capture more of the permutation invariance. Second, Figure 12 shows the contour map of $F^{(1)}$ in terms of the position of WEC 2 characterized by its $[x, y]$ coordinate. Here, WEC 3 moves symmetrically with respect to the $x$-axis, and to make sure the whole array is not symmetrical with respect to the $x$-axis, we set the distance of WEC 3 to the $x$-axis as $2/3$ of the corresponding distance of WEC 2 to the $x$-axis. In this case, if we reflect WEC 2 with respect to the $x$-axis, the whole layout of the array will also be reflected with respect to the $x$-axis. Based on the true function in Figure 12, we know the model response is symmetrical with respect to the $x$-axis. Again, the physics-constrained GP models perfectly capture the symmetry feature because of the use of kernels that

explicitly incorporate symmetry, while the standard GP model cannot capture the symmetry feature.

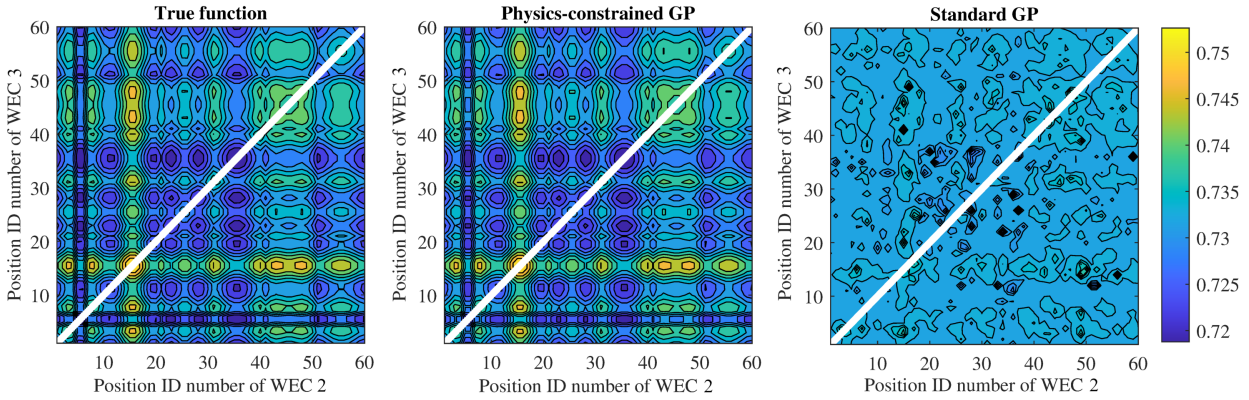


Figure 11: Permutation invariance of $F^{(1)}$ from true function, physics-constrained GP model, and standard GP model.

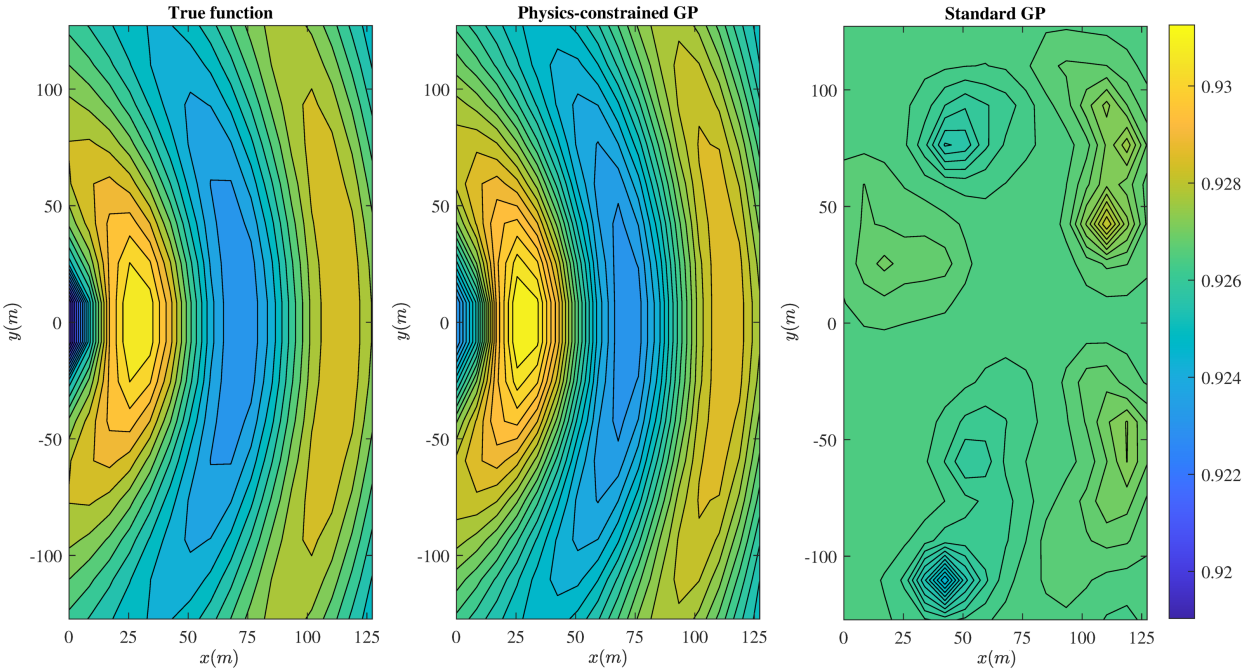


Figure 12: $x$-axis symmetry of $F^{(1)}$ from true function, physics-constrained GP model, and standard GP model.

Table 2 reports the accuracy metrics of the predictions from the physics-constrained GP model and the standard GP model. Note that the metrics are averaged over the elements of each hydrodynamic characteristics (i.e., $\mathbf{F}$, $\mathbf{a}$, and $\mathbf{b}$), and these hydrodynamic characteristics are calculated for $\omega = 0.6$ rad/s. The number of training data $n$ is again selected as 100, 120, 120, 120, 160, and 180 for 3-, 5-, 8-, 10-, 20-, and 30-WEC arrays, respectively. From Table 2, we can conclude that the physics-constrained GP model significantly outperforms the standard GP model in terms of the prediction accuracy, especially when the array has a large number of WECs. When the array has 3 WECs, the standard GP model trained with 100 data can also obtain a relatively good prediction. However, when the number of WECs in the array reaches

5, its prediction accuracy drops drastically, and 120 training data is not enough for a standard GP model to correctly learn the input-output relationship. Therefore, the standard GP model cannot explain the highly complex relationship with limited training data and also suffers severely from the curse of dimensionality. In comparison, for the physics-constrained GP model, the $R^2$ values calculated in all cases are close to 1, which indicates excellent prediction accuracy. This validates that encoding the invariance, symmetry, and additivity features into the kernel according to the input-output relationship can significantly improve the prediction accuracy. More importantly, with only 80 more training data sets, the prediction accuracy for 30 WECs almost does not change (or reduce) compared to that for 3 WECs, which means the prediction is less prone to the curse of dimensionality when wave frequency $\omega = 0.6$ rad/s. One possible reason is that using the physics-constrained kernel can build an interpretable GP model directly rather than learning the features from a large number of training data and thus can help reduce the required number of training data. Also, it has been proved that kernels that include lower-order additive structures sometimes allow us to make predictions over data far away from the training data (i.e., extrapolation) [33]. For example, additive kernels of first order give high covariance between model response at input locations that are similar in any one dimension. This is of significant importance to arrays with a large number of WECs, where the computational effort in running the MS solver is quite expensive and obtaining a large number of training data is sometimes impractical. Additionally, the results prove that the physics-constrained kernel has included the most contributed part of the model response (i.e., the first order of interaction), and this ensures that our computation in evaluating the proposed physics-constrained kernel can be efficient (i.e., no need to evaluate the kernel for the higher order of interactions where the evaluations are more expensive).

In addition to the comparison to the standard GP model, the proposed physics-constrained GP model is also compared to the hierarchical kriging model proposed in [14]. Table 2 reports the accuracy metrics of the predictions from hierarchical kriging model. Instead of using a single surrogate model to predict the hydrodynamic coefficients of the arrays with multiple WECs, the reference paper [14] constructs multiple surrogate models corresponding to clusters with fewer WECs. The prediction of the hydrodynamic coefficients is then obtained by summing the predictions from the hierarchical surrogate models according to the many-body expansion. The proposed surrogate models are also enhanced by taking into account the permutation invariance and symmetry features of the problem. Different from the physics-constrained GP model proposed in this study, the reference paper [14] encoded the physical knowledge though designing and transforming the surrogate model input. As can be seen from Table 2, the hierarchical kriging model accurately predicts all the hydrodynamic coefficients and, similar to the model proposed in this study, bypasses the curse of dimensionality. More importantly, the hierarchical surrogate models are established only for the 2-WEC and 3-WEC arrays, and no additional surrogate models are required to be constructed for arrays with any number of WECs in this example. By comparing the proposed physics-constrained GP model to the hierarchical surrogate model in [14], we can find that both models produce accurate predictions for arrays of 3 to 30 WECs. Therefore, in the context of hydrodynamic analysis (for array with relatively small number

| # of WECs | Physics-constrained GP model | | | Standard GP model | | | Hierarchical kriging model [14] | | |
|---|---|---|---|---|---|---|---|---|---|
| | **F** | **a** | **b** | **F** | **a** | **b** | **F** | **a** | **b** |
| 3 | 0.9992 | 0.9914 | 0.9929 | 0.7072 | 0.5696 | 0.5355 | 0.9999 | 0.9997 | 0.9998 |
| 5 | 0.9992 | 0.9866 | 0.9938 | 0.5342 | 0.3031 | 0.1781 | 0.9999 | 0.9998 | 0.9998 |
| 8 | 0.9988 | 0.9759 | 0.9928 | 0.3981 | 0.0000 | 0.0000 | 0.9999 | 0.9997 | 0.9997 |
| 10 | 0.9984 | 0.9714 | 0.9923 | 0.3847 | 0.0000 | 0.0000 | 0.9999 | 0.9997 | 0.9997 |
| 20 | 0.9971 | 0.9705 | 0.9935 | 0.3798 | 0.0000 | 0.0000 | 0.9999 | 0.9995 | 0.9996 |
| 30 | 0.9963 | 0.9687 | 0.9928 | 0.3130 | 0.0000 | 0.0000 | 0.9998 | 0.9991 | 0.9994 |

Table 2: Prediction accuracy metrics from physics-constrained GP model and standard GP model

of WECs), both the proposed physics-constrained GP model and the hierarchical surrogate model work well in predicting the hydrodynamic coefficients. On the other hand, they do have some differences in how the surrogate model is built. These differences may have impacts and implications on the computational effort and their accuracy, depending on the output of interest, wave conditions, the type of WECs, and size of arrays considered. The proposed physics-constrained GP model is constructed to predict the total response in an $N$-WEC array (i.e., hydrodynamic coefficients of each body), and one can choose the kernel and optimize the hyperparameters so that the model better fits the data for the interested response. Therefore, the training of the physics-constrained GP model aims to minimize the error for the total response. In comparison, the hierarchical surrogate model directly starts with the many-body expansion (i.e., the additive property) and builds kriging models for lower-order subsystems (i.e., 2- and 3-body interaction). Therefore, the hierarchical surrogate model aims to minimize the errors of the kriging models for the lower-order subsystems. To obtain the total response, one can predict the response from each subsystem using the kriging models and then add them. However, adding the predictions for the lower-order subsystems also means that the errors in these kriging models could be accumulated. If these kriging models have good accuracy, then the predicted total response may also have good accuracy; however, there is no explicit control over the error for the total response because the approach does not explicitly optimize for that. This might lead to large overall errors for the total response in some specific cases (e.g., for large-scale array where there are many combinations/terms to add, and/or when the accuracy of kriging models for lower-order subsystems is not high enough). Accordingly, there are respective implications on how expensive it is to build/train the surrogate models. For the proposed physics-constrained GP model, it would require running simulations and establishing training data for array size of interest. For large-scale array, the computational cost of establishing the training data could increase significantly. In comparison, the hierarchical surrogate model only requires running simulations and establishing training data for 2- and 3-WEC arrays. Therefore, it would have better scalability to large-scale array than the proposed physics-constrained GP model. More comprehensive comparisons between them related to the above discussed aspects as well as the validity and implications of the many-body expansion assumption will be carried out in future work.

### *4.5. Computational efficiency*

In this section, we discuss the efficiency gain provided by the physics-constrained GP model. On average, one evaluation of the numerical model for calculating the hydrodynamic characteristics of arrays of 3, 5, 8, 10, 20, and 30 WECs takes 0.1s, 0.5s, 2.1s, 4.1s, 23.2s, and 83.0s, respectively. Overall, the computational time increases dramatically with the number of WECs in the numerical model, further highlighting the computational challenges in modeling a large array. On the other hand, the physics-constrained GP model trained using selected $n$ training data to reach the targeted accuracy level (i.e., mean of $R^2$ over 0.98) takes only around 0.0003s, 0.0020s, 0.0135s, 0.0335s, 0.7166s, and 3.3s to obtain all the hydrodynamic characteristics when the considered wave frequency is $\omega = 0.6$ rad/s. Therefore, a speed-up of several orders of magnitude speedup can be obtained. Note that when more expensive numerical models (such as boundary element models) are used, the computational gain by using the physics-constrained model will be even greater.

## 5. Conclusions

This paper proposed a physics-constrained Gaussian process (GP) model to efficiently predict the hydrodynamic characteristics of WEC arrays with different numbers of WECs. Instead of building a standard GP model and learning the physical constraints (i.e., invariance, symmetry, and additivity features) of the WEC interaction problem through a large training data set, which is computationally inefficient or even prohibitive, the proposed physics-constrained GP model directly encodes these physical constraints/features into the model development. More specifically, the known physical constraints are encoded into the kernel by designing and integrating the invariant kernel and the additive kernel, and in this way a more "informative prior" can be provided for the GP model construction. Once trained, the physics-constrained GP model can be employed to directly and efficiently predict the hydrodynamic characteristics under different layouts.

Application to prediction of the hydrodynamic characteristics of arrays with different numbers of WECs demonstrates the high accuracy and efficiency of the proposed approach. The results show that the designed integrated kernel is able to correctly capture the invariance, symmetry, and additivity features of the problem. The proposed physics-constrained GP model can accurately predict the hydrodynamic characteristics with a relatively small number of training data, especially when the wave frequency is low. More importantly, the proposed physics-constrained GP model is much less vulnerable to the curse of dimensionality compared to the standard GP model, and such good scalability is crucial for analyzing arrays with a relatively large number of WECs.

One limitation of the proposed physics-constrained GP model is that if the decomposition of the many-body system does not converge fast (e.g., requires much more than first three orders of interaction), the computational cost of evaluating the proposed kernel might be high and thus it might take a longer time to train the GP model. Another limitation is that when the wave frequency is relatively large and input-output relationship shows strong non-linearity, a larger training set is needed to obtain the desired prediction

accuracy, which results in significant training cost. One potential remedy is to develop a sparse physics-constrained GP model, and future research will investigate the potential of such model. In addition, the application only investigated arrays with up to 30 WECs. Future research work will investigate the scalability of the proposed model to arrays of even larger sizes (e.g., with 40 to 100 WECs) by including cutoff distance and splitting the array into clusters. Another future research topic of interest is to use the hydrodynamic characteristics predicted by the proposed physics-constrained GP model to calculate the total power generation of the WEC array and also optimize the layout of the WEC array.

**Acknowledgements**

This research is supported in part by the National Science Foundation Engineering Design and System Engineering Program under grant number CMMI-2034040 and by the Colorado Energy Research Collaboratory Seed Grant Program. These supports are gratefully acknowledged.

This work was authored in part by the National Renewable Energy Laboratory, operated by Alliance for Sustainable Energy, LLC, for the U.S. Department of Energy (DOE) under Contract No. DE-AC36-08GO28308. Funding provided by the U.S. Department of Energy Office of Energy Efficiency and Renewable Energy Water Power Technologies Office. The views expressed in the article do not necessarily represent the views of the DOE or the U.S. Government. The U.S. Government retains and the publisher, by accepting the article for publication, acknowledges that the U.S. Government retains a nonexclusive, paid-up, irrevocable, worldwide license to publish or reproduce the published form of this work, or allow others to do so, for U.S. Government purposes.

**Appendix: Selection of parameters for the MS solver**

The parameters of the MS solver can be selected through a convergence study. More specifically, one can monitor the variation of hydrodynamic interactions concerning one parameter while keeping other parameters constant. The parameters can then be chosen so that the results stay unchanged (e.g., percentage change less than 1%). For example, when determining the order of interaction, the terms at which the eigenfunction series are truncated for the main fluid and the fluid below the body are first set separately to 20 and 50 (as proposed in [22]). The MS solver is then applied to calculate the hydrodynamic coefficients using a set of values for the interaction order. Note that the convergence study is performed on arrays with different numbers of WECs and specific configurations, and some examples can be found in [22]. As an example, here the convergence results for a selected 3-WEC array (with equal distances $L$ between the WECs) are shown. Different distances (i.e., $L = 3r_b$, $13r_b$, and $30r_b$) are considered as well. The variation of the hydrodynamic coefficients is shown in the first row of Figure 13. It is worth noting that the hydrodynamic coefficients are normalized to have values between 0 and 1. Also, the coefficients are grouped by physical meanings and then averaged over the same group for illustration, and the details about the grouping can

be found in Section 4.2. Similarly, the variation of the hydrodynamic coefficients concerning the other two parameters is also presented in Figure 13. From the figure we can observe that the hydrodynamic coefficients change significantly when the orders/parameters are small but reach plateau as the parameters increase to larger numbers. The parameters are finally chosen to ensure that all hydrodynamic coefficients remain unchanged. Many times more conservative choices are made for these parameters. More detailed discussion about determining these parameters in MS solver can be found in [34, 22].

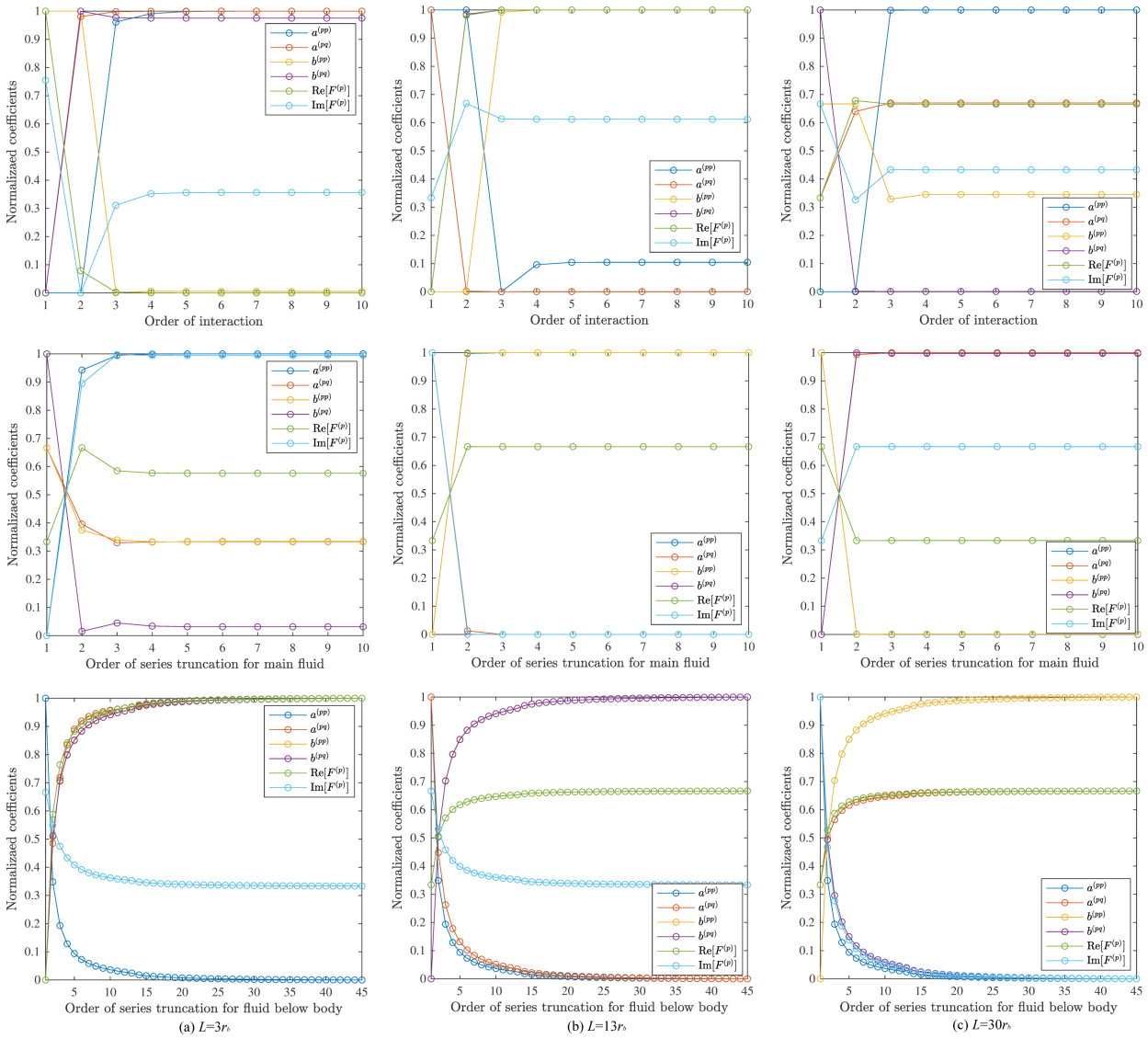


(a) $L$=3$r_b$ (b) $L$=13$r_b$ (c) $L$=30$r_b$

Figure 13: Convergence study of MS solver (shown for a selected 3-WEC array). The different columns show the results for different separation distances (i.e., $L$) between the WECs.

## References


[1] J. Scruggs, S. Lattanzio, A. Taflanidis, I. Cassidy, Optimal causal control of a wave energy converter in a random sea, Applied Ocean Research 42 (2013) 1–15.

[2] K. Budal, et al., Theory for absorption of wave power by a system of interacting bodies, Journal of Ship Research 21 (04) (1977) 248–254.

[3] B. Borgarino, A. Babarit, P. Ferrant, Impact of wave interactions effects on energy absorption in large arrays of wave energy converters, Ocean Engineering 41 (2012) 79–88.

[4] M. Göteman, Advances and challenges in wave energy park optimization-a review, Frontiers in Energy Research 8 (26).

[5] P. McIver, Wave interaction with arrays of structures, Applied Ocean Research 24 (3) (2002) 121–126.

[6] J. Falnes, Radiation impedance matrix and optimum power absorption for interacting oscillators in surface waves, Applied ocean research 2 (2) (1980) 75–80.

[7] P. McIver, Some hydrodynamic aspects of arrays of wave-energy devices, Applied Ocean Research 16 (2) (1994) 61–69.

[8] V. Twersky, Multiple scattering of radiation by an arbitrary configuration of parallel cylinders, The Journal of the Acoustical Society of America 24 (1) (1952) 42–46.

[9] J. Sacks, W. J. Welch, T. J. Mitchell, H. P. Wynn, Design and analysis of computer experiments, Statistical science (1989) 409–423.

[10] C. E. Rasmussen, Gaussian processes in machine learning, in: Advanced lectures on machine learning, Springer, 2004, pp. 63–71.

[11] G. Jia, A. Taflanidis, J. Scruggs, et al., Layout optimization of wave energy converters in a random sea, in: The Twenty-fifth International Ocean and Polar Engineering Conference, International Society of Offshore and Polar Engineers, 2015.

[12] M. Neshat, E. Abbasnejad, Q. Shi, B. Alexander, M. Wagner, Adaptive neuro-surrogate-based optimisation method for wave energy converters placement optimisation, in: International Conference on Neural Information Processing, Springer, 2019, pp. 353–366.

[13] D. Sarkar, E. Contal, N. Vayatis, F. Dias, Prediction and optimization of wave energy converter arrays using a machine learning approach, Renewable Energy 97 (2016) 504–517.

[14] J. Zhang, A. A. Taflanidis, J. T. Scruggs, Surrogate modeling of hydrodynamic forces between multiple floating bodies through a hierarchical interaction decomposition, Journal of Computational Physics 408 (2020) 109298.

[15] A. L. Frankel, R. E. Jones, L. P. Swiler, Tensor basis gaussian process models of hyperelastic materials, Journal of Machine Learning for Modeling and Computing 1 (1).

[16] G. E. Karniadakis, I. G. Kevrekidis, L. Lu, P. Perdikaris, S. Wang, L. Yang, Physics-informed machine learning, Nature Reviews Physics 3 (6) (2021) 422–440.

[17] B. Haasdonk, H. Burkhardt, Invariant kernel functions for pattern analysis and machine learning, Machine learning 68 (1) (2007) 35–61.

[18] S. Prakash, K. Mamun, F. Islam, R. Mudliar, C. Pau'u, M. Kolivuso, S. Cadralala, Wave energy converter: a review of wave energy conversion technology, in: 2016 3rd Asia-Pacific World Congress on Computer Science and Engineering (APWC on CSE), IEEE, 2016, pp. 71–77.

[19] B. Drew, A. R. Plummer, M. N. Sahinkaya, A review of wave energy converter technology, Proceedings of the Institution of Mechanical Engineers, Part A: Journal of Power and Energy 223 (8) (2009) 887–902.

[20] S. Mavrakos, P. Koumoutsakos, Hydrodynamic interaction among vertical axisymmetric bodies restrained in waves, Applied Ocean Research 9 (3) (1987) 128–140.

[21] S. Mavrakos, P. McIver, Comparison of methods for computing hydrodynamic characteristics of arrays of wave power devices, Applied Ocean Research 19 (5-6) (1997) 283–291.

[22] S. Mavrakos, Hydrodynamic coefficients for groups of interacting vertical axisymmetric bodies, Ocean Engineering 18 (5) (1991) 485–515.

[23] H.-H. Hsu, Y.-C. Wu, The hydrodynamic coefficients for an oscillating rectangular structure on a free surface with sidewall, Ocean Engineering 24 (2) (1997) 177–199.

[24] C. Audet, J. E. Dennis Jr, Analysis of generalized pattern searches, SIAM Journal on optimization 13 (3) (2002) 889–903.

[25] V. Picheny, D. Ginsbourger, O. Roustant, R. T. Haftka, N.-H. Kim, Adaptive designs of experiments for accurate approximation of a target region, Journal of Mechanical Design 132 (7) (2010) 071008.

[26] A. P. Bartók, R. Kondor, G. Csányi, On representing chemical environments, Physical Review B 87 (18) (2013) 184115.

[27] M. van der Wilk, M. Bauer, S. John, J. Hensman, Learning invariances using the marginal likelihood, in: Advances in Neural Information Processing Systems, 2018, pp. 9938–9948.

[28] M. S. Gordon, D. G. Fedorov, S. R. Pruitt, L. V. Slipchenko, Fragmentation methods: A route to accurate calculations on large systems, Chemical reviews 112 (1) (2011) 632–672.

[29] K. Yao, J. E. Herr, J. Parkhill, The many-body expansion combined with neural networks, The Journal of chemical physics 146 (1) (2017) 014106.

[30] S. N. Lophaven, H. B. Nielsen, J. Søndergaard, et al., DACE: a Matlab kriging toolbox, Vol. 2, Citeseer, 2002.

[31] D. Ginsbourger, O. Roustant, N. Durrande, Invariances of random fields paths, with applications in gaussian process regression, arXiv preprint arXiv:1308.1359.

[32] N. Durrande, D. Ginsbourger, O. Roustant, Additive covariance kernels for high-dimensional gaussian process modeling, in: Annales de la Faculté des sciences de Toulouse: Mathématiques, Vol. 21, 2012, pp. 481–499.

[33] D. Duvenaud, Automatic model construction with gaussian processes, Ph.D. thesis, University of Cambridge (2014).

[34] C. Garrett, Wave forces on a circular dock, Journal of Fluid Mechanics 46 (1) (1971) 129–139.